

# AN ABSTRACT OF THE THESIS OF

Douglas Edward Robertson for the Master of Science in Physical Science, Physics Emphasis presented in May 1995. Title: Photoelectric Heating of Interstellar Gas. Abstract approved: *Jorge Ballent*

The emission of photoelectrons from interstellar dust grains is thought to be the dominant mechanism by which stellar radiant energy is transferred to interstellar gas. The purpose of this theoretical research is to refine previous models of photoelectric heating.

The photoelectric emission rate is calculated for interstellar graphitic grains in a typical interstellar ultraviolet radiation field. The effect of the surface potential and photoelectron energy distribution is included. The free electron capture rate is calculated for several interstellar gas conditions as a function of temperature, electron density and grain charge. From the charge balance between photoemission and electron capture the grain charge distribution is obtained. The net heating rate is then calculated for appropriate grain sizes and a Mathis-Rumpl-Nordsieck size distribution of grains.

**Photoelectric Heating  
of  
Interstellar Gas**

**A Thesis**

**Presented to**

**the Division of Physical Sciences  
EMPORIA STATE UNIVERSITY**

**In Partial Fulfillment of  
the Requirements for the Degree  
Master of Science**

**by**

**Douglas Edward Robertson**

**May 1995**

*Dwayne Barkaus*  
Approved by the Major Division

*John E. Schuenem*  
Approved for the Graduate Council

*George Ballato*  
Committee Chairman

*Annelle Caly*  
Committee Member

*R. Jones*  
Committee Member

*Elizabeth Yanik*  
Committee Member

## **Acknowledgments**

I would like to express my deepest gratitude to Dr. Jorge Ballester for his guidance and supervision in the completion of this research. I would also like to thank Professor James Calvert, Dr. Robert Jones, Dr. Ron Keith, and Dr. Backhus for their invaluable advice and encouragement. I gratefully acknowledge the support of NASA/JOVE.

# Table of Contents

|                                  |     |
|----------------------------------|-----|
| Acknowledgments .....            | iii |
| Table of Contents .....          | iv  |
| List of Figures and Tables ..... | v   |
| Chapter 1. Introduction .....    | 1   |
| Chapter 2. Theory .....          | 6   |
| Chapter 3. Results .....         | 36  |
| Chapter 4. Conclusions .....     | 38  |
| References .....                 | 39  |
| Appendix A .....                 | 40  |
| Appendix B .....                 | 45  |
| Appendix C .....                 | 48  |
| Appendix D .....                 | 52  |
| Appendix E .....                 | 57  |
| Appendix F .....                 | 78  |

## List of Figures and Tables

|                 |    |
|-----------------|----|
| Figure 1 .....  | 58 |
| Figure 2 .....  | 59 |
| Figure 3 .....  | 60 |
| Figure 4 .....  | 61 |
| Figure 5 .....  | 62 |
| Figure 6 .....  | 63 |
| Figure 7 .....  | 64 |
| Figure 8 .....  | 65 |
| Figure 9 .....  | 66 |
| Figure 10 ..... | 67 |
| Figure 11 ..... | 68 |
| Figure 12 ..... | 69 |
| Figure 13 ..... | 70 |
| Figure 14 ..... | 71 |
| Figure 15 ..... | 72 |

|                        |           |
|------------------------|-----------|
| <b>Figure 16</b> ..... | <b>73</b> |
| <b>Figure 17</b> ..... | <b>74</b> |
| <b>Figure 18</b> ..... | <b>75</b> |
| <b>Figure 19</b> ..... | <b>76</b> |
| <b>Figure 20</b> ..... | <b>77</b> |
| <b>Table 1</b> .....   | <b>79</b> |
| <b>Table 2</b> .....   | <b>80</b> |
| <b>Table 3</b> .....   | <b>81</b> |

# Chapter 1

## Introduction

A major contribution to modern astrophysics has been the realization that the space between the stars is not devoid of matter. The study of the governing properties of this interstellar medium is of great interest. Interstellar gas is generally classified by its density, phase, and temperature. The density can range from approximately  $5 \times 10^3$  to more than  $1 \times 10^8$  particles per cubic meter. Hydrogen is the most abundant element throughout the universe. The resulting phase structure of the interstellar medium is characterized by a number of discrete components in which molecular ( $H_2$ ), atomic ( $HI$ ), or ionized ( $HII$ ) hydrogen predominates. Based on the three-phase model of Mckee and Ostriker<sup>1</sup> interstellar gas has four major components; cold molecular  $H_2$  ( $\approx 15 K$ ), cool atomic  $HI$  ( $\approx 80 K$ ), a warm mixture of  $HI$  and  $HII$  ( $\approx 8000 K$ ), and hot ionized  $HII$  ( $\approx 5 \times 10^5 K$ ) (Whittet)<sup>2</sup>.

The interstellar medium is thought to consist of low density, ionized, hot gas in which two distinct types of interstellar clouds reside. The first type is a *diffuse* cloud that is predominately cool atomic gas. The second is a *dense* cloud where molecular gas is surrounded by atomic gas. Both diffuse and dense clouds are immersed in the interstellar medium. The boundaries of the atomic and molecular components are called photodissociation regions. The clouds in the interstellar medium are maintained by pressure equilibrium. Although hydrogen is the major component of the interstellar clouds, assorted molecules and dust may also be present in the clouds. Interstellar clouds are



in a constant cycle of evolution. As the clouds evolve, they eventually contract into stars. Cloud temperatures of 100  $K$  or more must be the result of an energy exchange between the interstellar radiation field and the cloud constituents. Understanding this energy balance is significant in the quantitative theories of interstellar gas. Research shows that photoelectrons from dust grains may be the dominant heating source of the gas.

The three dust grain heating mechanisms by which energy can be transferred to the gas are collisions, chemical reactions, and photoelectron emissions. For heating due to collisions, energy from a nearby star must be absorbed by a grain. This absorbed energy will increase the average kinetic energy of the grain. In comparison to the other grains, this grain will now be warmer. When a cooler grain collides with a warmer one, energy will be transferred by conduction.

At the grain's surface the discharging of a negative grain by ion impact and the formation of molecular hydrogen may occur. Both of these chemical reactions are exothermic and some of this energy may penetrate the grain and heat it.

For grains in a region of significant ultraviolet  $UV$  photon flux, the absorption of these photons by dust grains may result in the emission of energetic electrons into the surrounding gas. As this occurs the grain is capturing electrons from the same surrounding gas. The energy of the photoelectrons is dependent upon the photon's energy, the grain's work function, and the grain's surface potential. The energy of the captured electrons only depends upon the free electron temperature of the surrounding

gas. Heating of this gas will occur if the energy of the emitted electrons is greater than the energy of the captured electrons.

Despite the importance of photoelectric heating, it is not well understood at a fundamental level (Bakes and Tielens)<sup>3</sup>. The interaction of electromagnetic radiation with particles that have sizes comparable to the radiation's wavelength is complicated. It becomes more complicated when considering particles of varying geometry and composition. Although the geometry and composition of interstellar dust is not certain, Mathis, Rumpl, and Nordseick<sup>4</sup> have shown that an average interstellar extinction curve can be reproduced by a power law distribution of spherical graphite and silicate grains. This distribution is now known as the *MRN* distribution. In this research we use Ding's<sup>5</sup> computed values for the photoelectric yields and absorption coefficients along with numerical methods to calculate both photoelectron emission and heating rates. The photoelectron emission rate will be balanced against the electron capture rate to determine the grain charge distribution. The difference between the photoelectric heating and particle capture cooling rates will determine a heating rate for each grain size. A *MRN* size distribution will be assumed in order to calculate the total photoelectric heating per hydrogen atom for the surrounding interstellar gas.

The photoelectric heating in the interstellar medium has been the subject of numerous investigations. Modeling photoelectric emission from interstellar grains is a fundamental question that is important in a variety of individual investigations. Published research has been in the form of a relatively small number of papers making fundamental contributions.

The 1978 work of Draine<sup>6</sup> has influenced all subsequent discussion of photoelectric heating. This fundamental paper established several features of the basic model. The enhanced photoelectric yield of small particles as compared to bulk materials was initially presented by Watson<sup>7</sup>. Combining this idea with laboratory measurements and general expectations Draine<sup>6</sup> developed a simplified photoelectric yield function. Draine<sup>6</sup> furthermore considered photoelectrons emitted with a range of kinetic energies, which is a necessary component in photoelectric calculations. Therefore, previous photoemission investigations by de Jong<sup>8</sup> were flawed by considering the photoelectrons as monoenergetic. Draine<sup>6</sup> also compiled both theoretical and measured data concerning the average *UV* background, and produced a simple analytical approximation. Draine<sup>6</sup> included the cooling of the surrounding gas by particle capture in his calculation, in contrast to the investigations by de Jong<sup>8</sup> and Jura<sup>9</sup>. Draine's<sup>6</sup> model was deliberately developed in a very general manner and therefore is open to several possible refinements. Nevertheless Draine's<sup>6</sup> photoelectric heating model set the theme for all recent investigations.

In 1987 Draine and Sutin<sup>10</sup> investigated collisional heating of interstellar gas clouds. In this case electron capture and ion capture are the only competing grain charging phenomena. Although photoelectric heating is not considered, their formulation of a charge probability distribution is directly applicable to the photoelectric case.

The most recent photoelectric heating investigation is the 1994 work of Bakes and Tielens<sup>3</sup>. Their work basically extends Draine's<sup>6</sup> investigation down to very small grains of molecular size. Grains with sizes above the

molecular domain are generally considered spherical whereas Bakes and Tielens<sup>3</sup> consider the molecular sized grains as polycyclic aromatic hydrocarbons *PAHs* in the form of circular disks. They consider a *MRN* size distribution with both varieties but conclude that doing so has virtually no effect on the total photoelectric heating rate.

The purpose of this theoretical research is to refine previous models of photoelectric heating. The principal refinements are improvements in the photoelectric yield function and the photoelectron kinetic energy spectrum. Although the fundamental theory is available in the published literature, it is distributed among several papers. Furthermore, many equations are presented with little or no derivation and their physical basis is not clear. A significant component of this research is to assemble the fundamental theory along with coherent derivations and clear physical bases.

In Chapter 2 we present the basic theory of photoelectric heating. Our results are presented in Chapter 3. Chapter 4 is a discussion of our conclusions. In Appendix A particle capture rates are formulated. Particle cooling rates are derived in Appendix B. Appendices C and D are program listings for the FORTRAN programs which were written to perform the necessary numerical calculations. Appendix E presents figures and graphs and Appendix F presents tabular data and information.

## Chapter 2

### Theory

#### 1. The Photoelectric Effect

Electrons are generally strongly bound in a solid by the surface potential barrier. If an electron has enough energy it may overcome the barrier and escape. An electron can gain the needed energy in a variety of ways.

If certain materials are irradiated by short wavelength (high energy) electromagnetic radiation, electrons will escape via the photoelectric effect. This process will only occur if the incident photons have energy greater than a specific threshold value known as the work function  $\phi_0$ , which is equal to the energy necessary for an electron to overcome the surface barrier. The kinetic energy  $E$  of the emitted photoelectron depends on the energy  $h\nu$  of the incident photon by

$$E = h\nu - \phi_0. \quad (1)$$

Not all materials will be subject to the photoelectric effect. Materials will exhibit the photoelectric effect when short wavelength photons are more energetic than the surface barrier. Generally these materials are good electrical conductors.

A spherical grain of radius  $a$  has a geometrical cross-section of  $\pi a^2$ . A detailed investigation into how electromagnetic radiation interacts with small particles will lead to the result that the cross-sectional area is not equal to the geometrical cross-section  $\pi a^2$  but given by  $Q\pi a^2$  (Evans)<sup>11</sup>. The quantity  $Q$  is known as the *optical efficiency*. The optical efficiency (which is  $\approx 1$ ) depends upon the nature of the grain (refractive index, size, etc.) and the wavelength of the radiation involved. Furthermore the radiation-grain interaction (extinction, scattering or absorption) must be specified because  $Q$  differs for each case. For photoelectric considerations the relevant radiation-grain interaction is the absorption of electromagnetic radiation, therefore  $Q_{abs}$  is the optical efficiency of interest. Throughout the remainder of this paper  $Q$  will be used with the understanding that  $Q_{abs}$  is intended.

Not every absorbed photon will produce a photoelectron. The process involves a quantity called the photoelectric yield  $Y$ , which is the number of photoelectrons per absorbed photon. The yield is dependent upon the nature of the grain and photon energy (Evans)<sup>12</sup>.

Consider a grain in a region of isotropic photon energy density  $u_\lambda$ . The photon energy per unit volume per wavelength interval is  $u_\lambda$ , therefore the number of photons per volume per wavelength interval is  $u_\lambda/(hc/\lambda)$ . In time  $dt$  the grain will absorb some fraction of all the photons within a sphere of radius  $cdt$  as depicted in Figure 1. In order to calculate the fraction absorbed consider a cylindrical surface of cross-sectional area  $Q\pi a^2$  and length  $cdt$  extending away from the grain. The direction of the cylinder is defined by the normal to the cross section  $\hat{n}$  as in Figure 2. The grain will absorb all photons within this cylinder with direction  $\hat{n}$ . Actually the absorbed photons'

directions are defined by a differential element of solid angle  $d\Omega$  which is centered about  $\hat{n}$ , as shown in Figure 3. The number of photons per solid angle per volume per wavelength interval is

$$\frac{1}{4\pi} \frac{u_\lambda}{(hc/\lambda)}. \quad (2)$$

The number of photons absorbed by the grain in time  $dt$  in a wavelength interval  $d\lambda$  and from direction within a solid angle  $d\Omega$  is

$$(\pi a^2)(cdt) \frac{1}{4\pi} \frac{u_\lambda d\lambda}{(hc/\lambda)} d\Omega. \quad (3)$$

Integrating over all possible directions introduces a factor  $4\pi$ . Integrating over all wavelengths, the number of photons absorbed per time is given by

$$\int (Q\pi a^2) \frac{u_\lambda \lambda d\lambda}{h}. \quad (4)$$

Multiplying this by the photoelectric yield gives the number of photoelectrons emitted per time  $J_{pe}$  as

$$J_{pe} = \int \frac{u_\lambda \lambda}{h} Q\pi a^2 Y d\lambda. \quad (5)$$

The range of integration begins from the photon wavelength with just enough energy to liberate an electron and ends with the photon wavelength with an

energy of  $13.6 \text{ eV}$ . The upper energy limit of  $13.6 \text{ eV}$  is due to the fact that hydrogen is the predominant constituent in the interstellar space and has an ionization energy of  $13.6 \text{ eV}$ . Any photon originating with energy greater than or equal to  $13.6 \text{ eV}$  will most likely use all or part of its energy to ionize interstellar hydrogen (Ballester, Shi, and Dwek)<sup>13</sup>. The lower limit can be chosen with knowledge of the photoelectric yield. The yield drops several orders of magnitudes from  $912 \text{ \AA}$  (photon wavelength with energy of  $13.6 \text{ eV}$ ) to  $1500 \text{ \AA}$ , therefore this will be the wavelength integration range. Tables 1 and 2 show the  $QY$  data calculated by Ding<sup>5</sup>. In Figure 4 Ding's data is compared to the simple function assumed by Draine.



## 2. Standard $UV$

The interstellar  $UV$  energy density  $u_\lambda$  has previously been theoretically modeled and measured for various photon energies below  $13.6 \text{ eV}$  by numerous researchers. Draine<sup>6</sup> has fit an average curve to this data to produce a “standard”  $UV$  spectrum  $F(E_\nu)$ . This standard  $UV$  spectrum is valid over the range 5 to  $13.6 \text{ eV}$  and the analytical expression is

$$F(E_\nu) = \left[ 1.658 \times 10^6 (E_\nu) - 2.152 \times 10^5 (E_\nu)^2 + 6.919 \times 10^3 (E_\nu)^3 \right] \text{photons cm}^{-2} \text{sr}^{-1} \text{eV}^{-1}. \quad (6)$$

$F(E_\nu)$  is the number photons incident per energy per area per time per solid angle. Since the expression in Equation 5 is per wavelength rather per energy, it is necessary to introduce an additional factor. Assuming an isotropic photon flux

$$4\pi F(E_\nu) dE_\nu = \frac{\lambda u_\lambda}{h} (-d\lambda). \quad (7)$$

Using  $E_\nu = hc/\lambda$ , one obtains  $dE_\nu = -(hc/\lambda^2)d\lambda$ . Therefore,

$$u_\lambda = \frac{4\pi h^2 c}{\lambda^3} F\left(\frac{hc}{\lambda}\right). \quad (8)$$

$F(E_\nu)$  is valid over the energy range 5 to  $13.6 \text{ eV}$ , this corresponds to the

wavelength range 2480 to 912 Å. The integration range for the number of photoelectrons emitted per time is 1500 to 912 Å, therefore the expression for  $u_\lambda$  in Equation 5 can be substituted into the integral. Doing so gives  $J_{pe}$  as

$$J_{pe} = \int \frac{4\pi hc}{\lambda^2} F\left(\frac{hc}{\lambda}\right) Q\pi a^2 Y d\lambda. \quad (9)$$

### 3. Grain Charge

When a grain loses a photoelectron it becomes positively charged ( $Z > 0$ ). The escaping photoelectron is attracted back to the grain due to Coulomb attraction. This increases the energy needed for the next electron to escape. This can be taken into account by adding a surface potential term to the work function to represent this added energy barrier seen by a photoelectron. The surface energy barrier becomes

$$\phi_0 + eU, \quad (10)$$

where  $U$  is the surface potential and

$$U = \frac{Ze}{4\pi\epsilon_0 a}. \quad (11)$$

Far from the grain, the energy of a photoelectron from a positive grain is

$$E = h\nu - \phi_0 - eU. \quad (12)$$

In other words, for a positive grain the maximum possible photoelectron energy is reduced by  $eU$ .

In some regions electron capture is large enough that there is a significant number of negatively charged grains. Therefore, it is necessary to consider photoemission from a negative grain ( $Z < 0$ ). Instead of an attractive

force, the photoelectron will be repelled from the negative grain. The net effect of negative grain is to increase the energy of the photoelectrons. Since  $Z$  is negative, the Equations 10 and 12 for the surface barrier and photoelectron energy are unchanged. In this case the maximum possible photoelectron energy is increased by  $-eU$ .

#### 4. Photoelectron Kinetic Energy Spectrum

Photoelectron energies range from zero to a maximum energy representing an electron just at the surface of the grain. Photoelectrons that are initially excited near the surface of the grain are expected to escape with the maximum possible energy. However, photoelectrons that are initially excited deep inside the grain may lose most of their energy during the escape process. The maximum energy after escape (i.e. far from the grain) is given by Equation 12 and the minimum energy is zero.

Figure 5 shows Feuerbacher and Fitton's<sup>14</sup> measured photoelectron energy spectrum for 12.4 eV photons incident on bulk graphite. The most energetic photoelectrons have an energy near 8 eV, that according to Equation 1 corresponds to  $\phi_0 = 4.4$  eV. Although this data is from bulk studies of graphite, it probably is representative of photoelectron kinetic energy spectra for graphite grains with radii considerably larger than the photoelectron escape length. In Ding's<sup>5</sup> calculations, an escape length of 10 Å is considered, therefore the bulk spectrum will be considered representative for graphite dust grains with radii greater than 20 Å. For grains with radii comparable to the escape length, the spectrum's peak is expected to shift towards higher energy as the base narrows. For molecular-sized grains, the photoelectrons may become monoenergetic, i.e. they all have the same energy.

In previous photoelectric models, simple spectra have been used to reduce the complexity of photoelectric calculations. Photoelectrons have

been assumed to be monoenergetic or to have a “box” spectrum. The box spectrum is compared to actual data in Figure 5. Also seen in Figure 5 is a “tent” function that is more representative of actual data but has not been previously considered. In the box and tent spectra we have used  $\phi_0 = 8 \text{ eV}$ . This choice was originally made by Draine<sup>6</sup> so that the box spectrum would have the same average energy as the measured spectrum. Keeping  $\phi_0 = 8 \text{ eV}$  for the tent distribution allows comparison with Draine’s result and clearly produces a better fit to the measured spectrum. Both energy spectrums will be considered throughout for completeness and comparative reasons. When the kinetic energy spectrum is considered the expression for the photoemission rate is

$$J_{pe} = \int \frac{4\pi hc}{\lambda^2} F\left(\frac{hc}{\lambda}\right) Q \pi a^2 Y d\lambda \int_0^{\infty} f(E) dE, \quad (13)$$

where  $f(E)$  is the normalized kinetic energy spectrum and  $f(E)dE$  is the fraction of all electrons ejected by a photon of wavelength  $\lambda$  that emerge with kinetic energy in the range  $E$  to  $E+dE$ . Each possible choice  $f(E)$  is normalized such that for a neutral grain

$$\int_0^{\infty} f(E) dE = 1. \quad (14)$$

Furthermore, the average photoelectron energy for a neutral grain must be

$$\int_0^{\infty} f(E) E dE = \frac{1}{2} (h\nu - \phi_0). \quad (15)$$

The normalized box function is defined as

$$f(E) = \begin{cases} \frac{1}{h\nu - \phi_0} & 0 < E < h\nu - \phi_0 \\ 0 & \text{otherwise} \end{cases} \quad (16)$$

for neutral grains,

$$f(E) = \begin{cases} \frac{1}{h\nu - \phi_0} & 0 < E < h\nu - \phi_0 - eU \\ 0 & \text{otherwise} \end{cases} \quad (17)$$

for positive grains, and

$$f(E) = \begin{cases} \frac{1}{h\nu - \phi_0} & -eU < E < h\nu - \phi_0 - eU \\ 0 & \text{otherwise} \end{cases} \quad (18)$$

for negative grains. The three cases are illustrated in Figures 6, 7, and 8.

The normalized tent function is

$$f(E) = \begin{cases} \frac{4E}{(h\nu - \phi_0)^2} & 0 < E < \frac{1}{2}(h\nu - \phi_0) \\ \frac{-4[E - (h\nu - \phi_0)]}{(h\nu - \phi_0)^2} & \frac{1}{2}(h\nu - \phi_0) < E < (h\nu - \phi_0) \end{cases} \quad (19)$$

for neutral grains,

$$f(E) = \begin{cases} \frac{4(E + eU)}{(h\nu - \phi_0)^2} & 0 < E < \frac{1}{2}(h\nu - \phi_0) - eU \\ \frac{-4[E - (h\nu - \phi_0 - eU)]}{(h\nu - \phi_0)^2} & \frac{1}{2}(h\nu - \phi_0) - eU < E < (h\nu - \phi_0) - eU \end{cases} \quad (20)$$

for positive grains, and

$$f(E) = \begin{cases} \frac{4(E + eU)}{(h\nu - \phi_0)^2} & eU < E < \frac{1}{2}(h\nu - \phi_0) - eU \\ \frac{-4[E - (h\nu - \phi_0 - eU)]}{(h\nu - \phi_0)^2} & \frac{1}{2}(h\nu - \phi_0) - eU < E < (h\nu - \phi_0) - eU \end{cases} \quad (21)$$

for negative grains. The three cases for the tent function are illustrated in Figures 9, 10, and 11.

In the expression for the photoemission rate

$$J_{pe} = \int \frac{4\pi hc}{\lambda^2} F\left(\frac{hc}{\lambda}\right) Q\pi a^2 Y d\lambda \int_0^{\infty} f(E) dE \quad (22)$$



the rightmost integration can be done analytically. After examining Figures 6 through 11, it can be seen that for both the normalized box and tent functions this integration is not equal to 1 when the grain is in a positive charge state. In a positive charge state some of the low energy photoelectrons will not have enough energy to escape the added attraction due to the surface potential. In the regions considered, photoemission dominates, therefore grains tend to be positive. Since grains will be in the positive charge state it is necessary to consider the case when  $\int_0^{\infty} f(E)dE < 1$ .

Integrating the normalized box kinetic energy spectrum over the relevant range gives

$$\int_0^{\infty} f(E)dE = \int_0^{h\nu - \phi_0 - eU} \frac{1}{h\nu - \phi_0} dE = \frac{h\nu - \phi_0 - eU}{h\nu - \phi_0}. \quad (23)$$

Converting into wavelength representation produces

$$\int_0^{\infty} f(E)dE = \frac{hc/\lambda - \phi_0 - eU}{hc/\lambda - \phi_0}. \quad (24)$$

Substituting this back into the Equation 22 gives the expression for the photoemission rate as

$$J_{pe} = \int \frac{4\pi hc}{\lambda^2} F\left(\frac{hc}{\lambda}\right) Q\pi a^2 Y \left[ \frac{hc/\lambda - \phi_0 - eU}{hc/\lambda - \phi_0} \right] d\lambda. \quad (25)$$

Inserting the normalized tent kinetic energy spectrum function into the integral over the relevant range gives

$$\int_0^{\infty} f(E)dE = \int_0^{\frac{1}{2}(h\nu-\phi_0)-eU} \frac{4(E+eU)}{(h\nu-\phi_0)^2} dE + \int_{\frac{1}{2}(h\nu-\phi_0)-eU}^{h\nu-\phi_0-eU} \frac{-4(E-h\nu+\phi_0+eU)}{(h\nu-\phi_0)^2} dE. \quad (26)$$

After integrating and wavelength conversion

$$\int_0^{\infty} f(E)dE = 1 - \frac{2(eU)^2}{(hc/\lambda - \phi_0)^2}. \quad (27)$$

This is true when the tent peak at  $E = (h\nu - \phi_0)/2 - eU$ , is greater than zero.

When the peak is less than zero,

$$\int_0^{\infty} f(E)dE = \int_0^{h\nu-\phi_0-eU} \frac{-4(E-h\nu+\phi_0+eU)}{(h\nu-\phi_0)^2} dE. \quad (28)$$

After integrating and wavelength conversion

$$\int_0^{\infty} f(E)dE = \frac{2(hc/\lambda - \phi_0 - eU)^2}{(hc/\lambda - \phi_0)^2}. \quad (29)$$

Substituting these back into Equation 22 gives the expression for the photoemission rate as

$$J_{pe} = \int \frac{4\pi hc}{\lambda^2} F\left(\frac{hc}{\lambda}\right) Q\pi\alpha^2 Y \left[ 1 - \frac{2(eU)^2}{\left(\frac{hc}{\lambda} - \phi_0\right)^2} \right] d\lambda \quad (30)$$

when the peak is greater than zero. When the peak is less than zero,

$$J_{pe} = \int \frac{4\pi hc}{\lambda^2} F\left(\frac{hc}{\lambda}\right) Q\pi\alpha^2 Y \left[ \frac{2\left(\frac{hc}{\lambda} - \phi_0 - eU\right)^2}{\left(\frac{hc}{\lambda} - \phi_0\right)^2} \right] d\lambda. \quad (31)$$

It is necessary to evaluate the photoemission rate integrals numerically.

The numerical methods will be discussed in Chapter 3.

## 5. Charge Balance

Photoelectron emission will not continue indefinitely. Charge balance will be reached between the charging mechanisms that make the grain positive and the charging mechanisms that make the grain negative. When a grain is immersed in interstellar gas it will be bombarded by electrons and ions. Some of the electrons may “stick” to the grain surface therefore making the grain negatively charged. The ions may not necessarily stick to the grain but may combine with surface electrons and “lift” them off. This will have the effect of making the grain positively charged.

Photoelectron emission and ion capture are the mechanisms for charging the grains positive and electron capture is the mechanism for charging the grains negative. Particle capture rates are formulated in Appendix A. The electron capture rate  $J_e$  for negative grains ( $Z < 0$ ) is

$$J_e = n_e S_e \pi a^2 \left( \frac{8kT}{\pi m_e} \right)^{\frac{1}{2}} e^{-\frac{Ze^2}{4\pi\epsilon_0 a kT}}. \quad (32)$$

The exponential decrease with  $Z$  is in response to the repelling Coulomb force between the like negative charges of the grain and electron. When the grain is positive ( $Z > 0$ ),  $J_e$  is

$$J_e = n_e S_e \pi a^2 \left( \frac{8kT}{\pi m_e} \right)^{\frac{1}{2}} \left( 1 + \frac{Ze^2}{4\pi\epsilon_0 a kT} \right). \quad (33)$$

The electron is attracted to the grain by the positive charge and therefore the capture rate increases linearly with  $Z$ .

The ion capture rate  $J_i$  for negative grains ( $Z < 0$ ) is

$$J_i = n_i S_i \pi a^2 \left( \frac{8kT}{\pi m_i} \right)^{\frac{1}{2}} \left( 1 - \frac{Ze^2}{4\pi\epsilon_0 a kT} \right). \quad (34)$$

The ion is attracted to the grain by the negative charge and therefore the capture rate increases linearly with  $Z$ . When the grain is positive ( $Z > 0$ ),  $J_i$  is

$$J_i = n_i S_i \pi a^2 \left( \frac{8kT}{\pi m_i} \right)^{\frac{1}{2}} e^{\frac{-Ze^2}{4\pi\epsilon_0 a kT}}. \quad (35)$$

As before, the exponential decrease with  $Z$  is in response to the repelling Coulomb force between the like positive charges of the grain and ion. In essence the capture cross-sections grow or diminish in response to the grain-particle charge configurations.

In the regions considered, the photoemission rate  $J_{pe}$  is several orders of magnitude larger than the ion capture rate  $J_i$ . Therefore  $J_i$  can virtually be ignored and the balance between  $J_{pe}$  and the electron capture  $J_e$  will determine the grain's charge state.

## 6. Charge Probability Distribution

Even though the charge on a particular grain varies with time, the distribution of charge states among all grains of a given radius can be time-independent. For the following, consider a large number of grains with the same radius  $a$ .

Following the analysis of Draine and Sutin<sup>10</sup>, let  $N(Z)$  be the total number of grains of radius  $a$  with charge  $Z$  and  $N(Z+1)$  be the total number of grains of radius  $a$  with charge  $Z+1$ . If  $N_{tot}$  is the total number of grains with radius  $a$ ,

$$N_{tot} = \sum_{Z=-\infty}^{\infty} N(Z). \quad (36)$$

$N(Z)J_{pe}(Z) + N(Z)J_i(Z)$  is the total number of grains charging from  $Z$  to  $Z+1$  per unit time, and  $N(Z+1)J_e(Z+1)$  is the total number of grains charging from  $Z+1$  to  $Z$  per unit time.

The grain charge distribution will reach a steady state when the total number of grains charging from  $Z$  to  $Z+1$  per time equals the total number of grains charging from  $Z+1$  to  $Z$  per time. The equation representing this balance is

$$N(Z)J_{pe}(Z) + N(Z)J_i(Z) = N(Z+1)J_e(Z+1). \quad (37)$$

Dividing both sides by  $N_{tot}$  and defining  $f(Z)$  and  $f(Z+1)$  as the probability of finding a grain with charge  $Z$  or  $Z+1$  respectively gives,

$$f(Z)[J_{pe}(Z) + J_i(Z)] = f(Z+1)J_e. \quad (38)$$

In order to obtain  $f(Z)$ , it is necessary to successively apply the following equations

$$f(Z > 0) = f(0) \prod_{Z'=1}^Z \left[ \frac{J_{pe}(Z'-1) + J_i(Z'-1)}{J_e(Z')} \right] \quad (39)$$

and

$$f(Z < 0) = f(0) \prod_{Z'=-Z}^{-1} \left[ \frac{J_e(Z'+1)}{J_{pe}(Z') + J_i(Z')} \right]. \quad (40)$$

The multiplicative constant  $f(0)$  is determined by the normalization condition

$$\sum_{-\infty}^{\infty} f(Z) = 1. \quad (41)$$

Photoemission and ion capture work together to charge the grain positive. In the environments considered photoemission is dominant over ion capture, therefore ion capture is ignored. The equations for the charge probability distribution become

$$f(Z > 0) = f(0) \prod_{Z'=1}^Z \left[ \frac{J_{pe}(Z'-1)}{J_e(Z')} \right] \quad (42)$$

and

$$f(Z < 0) = f(0) \prod_{Z'=Z}^{-1} \left[ \frac{J_e(Z'+1)}{J_{pe}(Z')} \right]. \quad (43)$$



## 7. Heating and Cooling Rates

When a photoelectron is emitted into the surrounding gas its energy is transferred to the gas. The rate at which energy is delivered to the gas by a grain of radius  $a$  per time via photoemission is the heating rate  $H_{pe}$  and is given by

$$H_{pe} = \int \frac{4\pi hc}{\lambda^2} F\left(\frac{hc}{\lambda}\right) Q\pi a^2 Y d\lambda \int_0^{\infty} f(E) E dE. \quad (44)$$

Again the right most integration can be done analytically. For the normalized box function

$$\int_0^{\infty} f(E) E dE = \int_0^{hv - \phi_0 - eU} \frac{E}{hv - \phi_0} dE = \frac{1}{2} \frac{(hv - \phi_0 - eU)^2}{hv - \phi_0}. \quad (45)$$

Converting Equation 45 into wavelength representation gives

$$\int_0^{\infty} f(E) E dE = \frac{1}{2} \frac{(hc/\lambda - \phi_0 - eU)^2}{hc/\lambda - \phi_0}. \quad (46)$$

Substituting back into Equation 44 gives  $H_{pe}$  as

$$H_{pe} = \int \frac{4\pi hc}{\lambda^2} F\left(\frac{hc}{\lambda}\right) Q\pi a^2 Y \left[ \frac{1}{2} \frac{(hc/\lambda - \phi_0 - eU)^2}{hc/\lambda - \phi_0} \right] d\lambda. \quad (47)$$

For the normalized tent function with the peak greater than zero

$$\int_0^{\infty} f(E)EdE = \int_0^{\frac{1}{2}(h\nu - \phi_0) - eU} \frac{4(E + eU)E}{(h\nu - \phi_0)^2} dE + \int_{\frac{1}{2}(h\nu - \phi_0) - eU}^{h\nu - \phi_0 - eU} \frac{-4(E - h\nu + \phi_0 + eU)E}{(h\nu - \phi_0)^2} dE. \quad (48)$$

Carrying out the integration and converting into wavelength representation gives

$$\int_0^{\infty} f(E)EdE = \frac{4(eU)^3 + 3\left(\frac{hc}{\lambda} - \phi_0\right)^3 - 6eU\left(\frac{hc}{\lambda} - \phi_0\right)^2}{6\left(\frac{hc}{\lambda} - \phi_0\right)^2}. \quad (49)$$

When the peak is less than zero

$$\int_0^{\infty} f(E)EdE = \int_0^{h\nu - \phi_0 - eU} \frac{-4(E - h\nu + \phi_0 + eU)E}{(h\nu - \phi_0)^2} dE. \quad (50)$$

After integrating and converting Equation 50 into wavelength representation gives

$$\int_0^{\infty} f(E)EdE = \frac{2}{3} \frac{\left(\frac{hc}{\lambda} - \phi_0 - eU\right)^3}{\left(\frac{hc}{\lambda} - \phi_0\right)^2}. \quad (51)$$

Substituting these back into the Equation 44 gives  $H_{pe}$  as

$$H_{pe} = \int \frac{4\pi hc}{\lambda^2} F\left(\frac{hc}{\lambda}\right) Q\pi a^2 Y \left[ \frac{4(eU)^3 + 3\left(\frac{hc}{\lambda} - \phi_0\right)^3 - 6eU\left(\frac{hc}{\lambda} - \phi_0\right)^2}{6\left(\frac{hc}{\lambda} - \phi_0\right)^2} \right] d\lambda \quad (52)$$

when the peak is greater than zero. When the peak is less than zero,

$$H_{pe} = \int \frac{4\pi hc}{\lambda^2} F\left(\frac{hc}{\lambda}\right) Q\pi a^2 Y \left[ \frac{2\left(\frac{hc}{\lambda} - \phi_0 - eU\right)^3}{3\left(\frac{hc}{\lambda} - \phi_0\right)^2} \right] d\lambda. \quad (53)$$

It is necessary to evaluate these energy rate integrals numerically. The numerical methods will be discussed in Chapter 3.

The rates at which energy is transferred to the grains by particle capture are  $C_e$  and  $C_i$ , where these are the cooling rates from electron capture and ion capture respectively. The cooling rates are formulated in Appendix B. The cooling rate per charge by electron capture  $C_e$  on a negative grain ( $Z < 0$ ) is

$$C_e = n_e S_e \pi a^2 \left[ \frac{(2kT)^3}{\pi m_e} \right]^{\frac{1}{2}} \left( 2 - \frac{Ze^2}{4\pi\epsilon_0 a kT} \right) e^{\frac{Ze^2}{4\pi\epsilon_0 a kT}}. \quad (54)$$

The exponential decrease with  $Z$  is in response to the repelling Coulomb force between the like negative charges of the grain and electron. When the grain is positive ( $Z > 0$ ),  $C_e$  is

$$C_e = n_e S_e \pi a^2 \left[ \frac{(2kT)^3}{\pi m_e} \right]^{\frac{1}{2}} \left( 2 + \frac{Ze^2}{4\pi\epsilon_0 a k T} \right). \quad (55)$$

The electron is attracted to the grain by the positive and therefore the cooling rate increases linearly with  $Z$ .

For ion capture by a negative grain ( $Z < 0$ ),  $C_i$  is

$$C_i = n_i S_i \pi a^2 \left[ \frac{(2kT)^3}{\pi m_i} \right]^{\frac{1}{2}} \left( 2 - \frac{Ze^2}{4\pi\epsilon_0 a k T} \right). \quad (56)$$

Since  $Z < 0$ , this rate will grow linearly with  $Z$  due to Coulomb attraction. For a positive grain ( $Z > 0$ )  $C_i$  is given by

$$C_i = n_i S_i \pi a^2 \left[ \frac{(2kT)^3}{\pi m_i} \right]^{\frac{1}{2}} \left( 2 + \frac{Ze^2}{4\pi\epsilon_0 a k T} \right) e^{\frac{-Ze^2}{4\pi\epsilon_0 a k T}}. \quad (57)$$

The exponential decrease with  $Z$  is due to Coulomb repulsion.

Taking the difference between the heating and cooling rates will give an energy rate per charge per grain size. Multiplying by the known charge probability distribution and summing up the results will give a net energy rate per grain size. For a steady state charge distribution there is a net energy

transfer. In the interstellar regions considered, heating rates are greater than the cooling rates, therefore net heating of the gas occurs. Also of note is the result that in regions with significant *UV* fluxes, photoemission is dominant over electron capture. Therefore the grain charge distribution is dominated by positive charges. Since the ion cooling rate decreases exponentially with *Z* for positive grains, it can virtually be ignored.

## 8. Grain Size Distribution

Mathis, Rumpl, and Nordsieck<sup>4</sup> have shown that an “average” interstellar extinction curve can be reproduced by a mixture of two grain populations. The two grain populations are spherical graphite and silicate grains. In the *MRN* size distribution, the number of grains per unit volume having radius in the range  $a$  to  $a + da$ , is of the form

$$n(a)da \propto a^{-3.5} da. \quad (58)$$

This is close to that which is characteristic of grain-grain collisions (Evans)<sup>15</sup>. It is not thought that grain populations are dense enough in interstellar space for this “collisional” distribution to arise. This suggests that grains form in the environments of stars and are then ejected into interstellar space after the size distribution is established.

## **9. Interstellar Environments**

The two environments that will be considered in this research are a cool atomic cloud and a warm intercloud medium. Interstellar gas parameters are generally its density, phase, and temperature. Although exact values are not known for these parameters, theoretical values have been calculated. The parameters for these environments are taken from Bakes and Tielens<sup>3</sup>, for comparative purposes, and are given in Table 3.

## 10. Numerical Methods

The photoemission rate integral for the normalized box photoelectron kinetic energy spectrum is

$$J_{pe} = \int \frac{4\pi hc}{\lambda^2} F\left(\frac{hc}{\lambda}\right) Q\pi\alpha^2 Y \left[ \frac{hc/\lambda - \phi_0 - eU}{hc/\lambda - \phi_0} \right] d\lambda. \quad (59)$$

For the normalized tent kinetic energy spectrum there are two expressions for the photoemission rate,

$$J_{pe} = \int \frac{4\pi hc}{\lambda^2} F\left(\frac{hc}{\lambda}\right) Q\pi\alpha^2 Y \left[ 1 - \frac{2(eU)^2}{(hc/\lambda - \phi_0)^2} \right] d\lambda \quad (60)$$

when the tent peak  $E = (h\nu - \phi_0)/2 - eU$  is greater than zero, and

$$J_{pe} = \int \frac{4\pi hc}{\lambda^2} F\left(\frac{hc}{\lambda}\right) Q\pi\alpha^2 Y \left[ \frac{2(hc/\lambda - \phi_0 - eU)^2}{(hc/\lambda - \phi_0)^2} \right] d\lambda \quad (61)$$

when the peak is less than zero.

The heating rate integral for the box function is



$$H_{pe} = \int \frac{4\pi hc}{\lambda^2} F\left(\frac{hc}{\lambda}\right) Q\pi a^2 Y \left[ \frac{1}{2} \frac{(hc/\lambda - \phi_0 - eU)^2}{hc/\lambda - \phi_0} \right] d\lambda. \quad (62)$$

The heating rate for the tent function is

$$H_{pe} = \int \frac{4\pi hc}{\lambda^2} F\left(\frac{hc}{\lambda}\right) Q\pi a^2 Y \left[ \frac{4(eU)^3 + 3(hc/\lambda - \phi_0)^3 - 6eU(hc/\lambda - \phi_0)^2}{6(hc/\lambda - \phi_0)^2} \right] d\lambda, \quad (63)$$

when the peak is greater than zero, and

$$H_{pe} = \int \frac{4\pi hc}{\lambda^2} F\left(\frac{hc}{\lambda}\right) Q\pi a^2 Y \left[ \frac{2}{3} \frac{(hc/\lambda - \phi_0 - eU)^3}{(hc/\lambda - \phi_0)^2} \right] d\lambda, \quad (64)$$

when the peak is less than zero.

The FORTRAN program JHPEBOX.FOR calculates both the photoemission and heating rate integrals for the box function. The program takes  $QY$  data from Ding's<sup>5</sup> calculations (see Tables 1 and 2 for the tabular form of the data) and produces an output data file JHPEBOX.DAT which contains the photoemission rate  $J_{pe}$  versus grain charge  $Z$  for grains ranging in radius from 20 to 5000 Å. The FORTRAN program JHPETENT.FOR calculates both the photoemission and heating rate integrals for the tent function. This program takes the same  $QY$  data as input and outputs the data file JHPETENT.DAT in the same form as JHPEBOX.DAT. Considering that

the  $QY$  data of Ding<sup>5</sup> are in tabular form, sufficient accuracy is obtained by calculating all integrals numerically using the *trapezoidal rule* algorithm.

## Chapter 3

### Results

The calculation of  $J_{pe}$  and  $H_{pe}$  according to Equations 13 and 44 depends on the assumed grain optical efficiency, photoelectric yield,  $UV$  background, photoelectron kinetic energy spectrum, and charge state. The calculation of  $J_e$  depends on the assumed free electron density, gas temperature, and grain charge state.  $J_{pe}$  and  $H_{pe}$  are independent of the interstellar gas parameters and therefore are calculated once for all plausible grain charges.

The FORTRAN programs JHPEBOX.FOR and JHPETENT.FOR use the trapezoidal approximation algorithm to calculate  $J_{pe}$  and  $H_{pe}$  for the normalized box and tent functions respectively. The output file is imported into a spreadsheet where further calculations, such as  $J_e$  and  $C_e$ , are carried out. The complete program listing for JHPEBOX.FOR is in Appendix C and the listing for JHPETENT.FOR is in Appendix D.

The temperatures and electron densities used in this research are  $T = 100 K$ ,  $n_e = 7500 m^{-3}$  for cool atomic clouds and  $T = 8000 K$ ,  $n_e = 2500 m^{-3}$  for warm clouds as discussed in Chapter 1, Section 9. The grain sizes considered are 20, 30, 50, 70, 100, 150, 200, 300, 500, 700, 1000, 1500, 2000, 3000, and 5000  $\text{\AA}$ . Typical results are presented for 100  $\text{\AA}$  grains in both interstellar environments. In each case results from both the box and tent functions are presented.

$J_{pe}$  and  $J_e$  as functions of grain charge are presented in Figures 12 and 13. The charge probability distributions are presented in Figures 14 and 15. The net heating rate per grain,  $H_{pe} - C_e$ , is presented as a function of grain charge in Figures 16 and 17. The net heating rate per grain radius interval as a function of grain radius is presented in Figures 18 and 19. The best fits to the log-log graphs give a power law relation between heating rate and grain size approximately proportional to  $a^{-1.5}$ .

The net heating rates per grain size in Figures 18 and 19 were integrated from 20 to 5000  $\text{\AA}$  to give total heating rates. For the cool atomic clouds the total heating rate is  $7.68 \times 10^{-16} \text{ eV s}^{-1} (\text{H atom})^{-1}$  for the box distribution and  $7.64 \times 10^{-16} \text{ eV s}^{-1} (\text{H atom})^{-1}$  for the tent distribution. For the warm interclouds the total heating rate is  $1.32 \times 10^{-16} \text{ eV s}^{-1} (\text{H atom})^{-1}$  for the box distribution and  $5.90 \times 10^{-17} \text{ eV s}^{-1} (\text{H atom})^{-1}$  for the tent distribution. Using the approximate power law best fits the net heating rates per grain size have been extrapolated the down to 5  $\text{\AA}$  grains. For the cool atomic clouds the extrapolated total heating rate is  $1.95 \times 10^{-15} \text{ eV s}^{-1} (\text{H atom})^{-1}$  for the box distribution and  $1.93 \times 10^{-15} \text{ eV s}^{-1} (\text{H atom})^{-1}$  for the tent distribution. For the warm interclouds the extrapolated total heating rate is  $3.03 \times 10^{-16} \text{ eV s}^{-1} (\text{H atom})^{-1}$  for the box distribution and  $1.15 \times 10^{-16} \text{ eV s}^{-1} (\text{H atom})^{-1}$  for the tent distribution.

## Chapter 4

### Conclusions

In typical interstellar conditions, there is a net heating effect due to the emission of photoelectrons. In typical warm interstellar conditions the net heating rate becomes negative for temperatures above 8000  $K$ . Based on this result clouds with temperatures much greater than 8000  $K$  are not expected.

For both the box and tent photoelectron energy distributions the net heating rate is lower than the recent calculations of Bakes and Tielens<sup>3</sup>. This is mainly due to the different photoelectric yield function and optical efficiency being used.

The tent net heating rate is always less than the box net heating rate. This difference appears to be greatest when the net heating rate is close to zero. Extrapolating the heating rate per grain radius from 20  $\text{\AA}$  down to 5  $\text{\AA}$  increases the total net heating rate approximately by a factor of 2. Approximately 90% of the heating comes from grains with radii  $a \leq 100 \text{\AA}$ .

## REFERENCES

1. C.F. McKee and J.P. Ostriker, **Ap. J.**, **218**, 148 (1977).
2. D.C.B. Whittet, *Dust in the Galactic Environment*. (IOP, London, 1992), p.18.
3. E.L.O. Bakes and A.G.G.M. Tielens, **Ap. J.**, **427**, 822 (1994).
4. J.S. Mathis, W. Rumpl, and K.H. Nordsieck, **Ap. J.** **217**, 425 (1977).
5. Y. Ding, *Photoelectric Yield Enhancement of Small Graphite and Silicate Dust Grains*. (Thesis, Emporia State University, 1994).
6. B.T. Draine, **Ap. J. S. S.**, **36**, 595 (1978).
7. W.D. Watson, **Ap. J.**, **176**, 103 (1972).
8. T. de Jong, **Astr. Ap.**, **55**, 137 (1977).
9. M. Jura, **Ap. J.**, **191**, 375 (1976).
10. B.T. Draine and B. Sutin, **Ap. J.**, **320**, 803 (1987).
11. A. Evans, *The Dusty Universe*. (Ellis Horwood, Chichester, 1993), p.46.
12. A. Evans, *The Dusty Universe*. (Ellis Horwood, Chichester, 1993), p.60.
13. J.L. Ballester, Y. Shi, and E. Dwek, **J. Opt. Soc. Am. B**, in press (1995).
14. B. Feuerbacher and B. Fitton **Appl. Phys.**, **43**, 1563 (1972).
15. A. Evans, *The Dusty Universe*. (Ellis Horwood, Chichester, 1993), p.117.

# APPENDIX A

## Particle Capture Rates

(1) Positive ion captured by a positive dust grain.

Consider a positive ion of charge  $+e$  impacting a dust grain of radius  $a$ . The ion speed far from the grain is  $v_i$ , its speed on impact is  $V_i$ , and its impact parameter is  $b$ , as shown on Figure 20. Using the principle of conservation of energy

$$\frac{1}{2} m_i v_i^2 = \frac{1}{2} m_i V_i^2 + \frac{Ze^2}{4\pi\epsilon_0 a}. \quad (\text{A1})$$

The left side of Equation A1 is the energy of the ion at infinity, the right hand side is the energy of the ion at the surface of the grain at impact. Solving for the impact velocity gives

$$V_i = \left[ \frac{2}{m_i} \left( \frac{1}{2} m_i v_i^2 - \frac{Ze^2}{4\pi\epsilon_0 a} \right) \right]^{\frac{1}{2}}. \quad (\text{A2})$$

In order to determine the ion capture cross section it is necessary to consider the case of an ion which just grazes the grain surface see Figure 20. For this case the conservation of angular momentum states

$$bv_i = aV_i. \quad (\text{A3})$$

The left hand side of Equation A3 is the angular momentum at infinity, the right hand side is the angular momentum at the grain's surface. Solving for  $b$ , squaring, and multiplying by  $\pi$  gives

$$\pi b^2 = \pi a^2 \left( 1 - \frac{2Ze^2}{4\pi\epsilon_0 a m_i v_i^2} \right) = \sigma_i, \quad (\text{A4})$$

where  $\sigma_i$  is the ion-grain collision cross-section. Due to the ion-grain repulsion, there is a minimum velocity required for impact. Therefore the cross section will go to zero when

$$v_i = \left( \frac{2Ze^2}{4\pi\epsilon_0 a m_i} \right)^{\frac{1}{2}} = v_0. \quad (\text{A5})$$

The rate (number per time) at which ions with velocity  $v_i$  strike the grain is

$$n_i \sigma_i v_i, \quad (\text{A6})$$

where  $n_i$  is the ion number density. Not all ions that strike the grain's surface will remain, some may be reflected. The probability of an ion "sticking" to the grain's surface is called the *sticking coefficient*  $S_i$ . Taking the sticking coefficient  $S_i$  into consideration, the rate at which ions strike the grain becomes



$$n_i \sigma_i v_i S_i. \quad (\text{A7})$$

The sticking coefficient is probably dependent upon the energy of the approaching ion, grain composition, radius, and charge (Draine and Sutin)<sup>10</sup>. However detailed investigation into the sticking coefficient is unavailable and is usually assumed independent of velocity.

Integrating over the Maxwell speed distribution for all velocities, the ion capture rate  $J_i$  for positive grains ( $Z > 0$ ) is

$$J_i = n_i S_i \int_{v_0}^{\infty} \sigma_i v_i f(v_i) dv_i, \quad (\text{A8})$$

where the Maxwell speed distribution is given by

$$f(v_i) = 4\pi \left( \frac{m}{2\pi kT} \right)^{\frac{3}{2}} e^{-\frac{mv^2}{2kT}} v^2. \quad (\text{A9})$$

Inserting the known quantities into the equation,  $J_i$  becomes

$$J_i = n_i S_i 4\pi^2 a^2 \left( \frac{m_i}{2\pi kT} \right)^{\frac{3}{2}} \int_{v_0}^{\infty} \left( 1 - \frac{2Ze^2}{4\pi\epsilon_0 a m_i v_i^2} \right) v^3 e^{-\frac{mv_i^2}{2kT}} dv_i. \quad (\text{A10})$$

Making the substitution  $x = \frac{m_i v_i^2}{2kT}$  and integrating,  $J_i$  for positive grains is

$$J_i = n_i S_i \pi a^2 \left( \frac{8kT}{\pi m_i} \right)^{\frac{1}{2}} e^{\frac{-Ze^2}{4\pi\epsilon_0 a kT}}. \quad (\text{A11})$$

For a positive grain ( $Z > 0$ ), the ion capture rate decreases exponentially with  $Z$  due to Coulomb repulsion. From Equation A11 it can be concluded that the particle capture rate decreases in an exponential fashion when the particle and the grain have the same charge state. Therefore the electron capture rate  $J_e$  for negative grains ( $Z < 0$ ) is

$$J_e = n_e S_e \pi a^2 \left( \frac{8kT}{\pi m_e} \right)^{\frac{1}{2}} e^{\frac{Ze^2}{4\pi\epsilon_0 a kT}}. \quad (\text{A12})$$

(2) Electron capture by a positive dust grain.

The steps are similar to the ones considered for the ion captured by a positive grain. The differing aspect is the energy of the particle at impact. The energy conservation equation is

$$\frac{1}{2} m_e v_e^2 = \frac{1}{2} m_e V_e^2 - \frac{Ze^2}{4\pi\epsilon_0 a}. \quad (\text{A13})$$

Which will lead to an electron-grain cross-section of

$$\pi b^2 = \pi a^2 \left( 1 + \frac{2Ze^2}{4\pi\epsilon_0 a m_e v_e^2} \right) = \sigma_e. \quad (\text{A14})$$

This cross section is greater than the geometric area  $\pi a^2$  for all  $Z$ .  
Substituting this cross-section into

$$J_e = n_e S_e \int_0^{\infty} \sigma_e v_e f(v_e) dv_e, \quad (\text{A15})$$

gives

$$J_e = n_e S_e 4\pi^2 a^2 \left( \frac{m_e}{2\pi kT} \right)^{\frac{3}{2}} \int_0^{\infty} \left( 1 + \frac{2Ze^2}{4\pi\epsilon_0 a m_e v_e^2} \right) v^3 e^{-\frac{mv_e^2}{2kT}} dv_e. \quad (\text{A16})$$

Making the substitution  $x = \frac{m_e v_e^2}{2kT}$  and integrating,  $J_e$  for positive grains is

$$J_e = n_e S_e \pi a^2 \left( \frac{8kT}{\pi m_e} \right)^{\frac{1}{2}} \left( 1 + \frac{Ze^2}{4\pi\epsilon_0 a kT} \right). \quad (\text{A17})$$

For a positive grain ( $Z > 0$ ), the electron capture rate increases linearly with  $Z$  due to Coulomb attraction. From Equation A17 it can be concluded that the particle rate should increase in a linear fashion with  $Z$  when the particle and the grain have opposite charge states. Therefore  $J_i$  for negative grains ( $Z < 0$ ) is

$$J_i = n_i S_i \pi a^2 \left( \frac{8kT}{\pi m_i} \right)^{\frac{1}{2}} \left( 1 - \frac{Ze^2}{4\pi\epsilon_0 a kT} \right). \quad (\text{A18})$$

## APPENDIX B

### Particle Cooling Rates

(1) Positive ion captured by a positive dust grain.

The procedure follows (1) in Appendix A step by step until the integration. The energy of the ion is of interest, therefore the ion cooling rate  $C_i$  is given by

$$C_i = n_i S_i \int_{v_0}^{\infty} \sigma_i v_i f(v_i) E_i dv_i, \quad (\text{B1})$$

where  $E_i = (1/2)m_i v_i^2$ . Inserting the known quantities into the equation,  $C_i$  becomes

$$C_i = n_i S_i 4\pi^2 a^2 \left( \frac{m_i}{2\pi kT} \right)^{3/2} \int_{v_0}^{\infty} \left[ \left( 1 - \frac{2Ze^2}{4\pi\epsilon_0 a m_i v_i^2} \right) v^3 e^{-\frac{mv_i^2}{2kT}} \right] \frac{1}{2} m_i v_i^2 dv_i. \quad (\text{B2})$$

Making the substitution  $x = \frac{m_i v_i^2}{2kT}$  and integrating,  $C_i$  for positive grains is

$$C_i = n_i S_i \pi a^2 \left[ \frac{(2kT)^3}{\pi m_i} \right]^{1/2} \left( 2 + \frac{Ze^2}{4\pi\epsilon_0 a kT} \right) e^{-\frac{Ze^2}{4\pi\epsilon_0 a kT}}. \quad (\text{B3})$$

From Equation B3 it can be concluded that the particle cooling rate decreases in an exponential fashion with  $Z$  (although the linear term is increasing, the decreasing exponent is dominant) when the particle and the grain have the same charge state,. Therefore the electron cooling rate  $C_e$  for negative grains ( $Z < 0$ ) is

$$C_e = n_e S_e \pi a^2 \left[ \frac{(2kT)^3}{\pi m_e} \right]^{\frac{1}{2}} \left( 2 - \frac{Ze^2}{4\pi\epsilon_0 a kT} \right) e^{\frac{Ze^2}{4\pi\epsilon_0 a kT}}. \quad (\text{B4})$$

(2) Electron capture by a positive dust grain.

The procedure follows (2) in Appendix A step by step until the integration. Again, the energy of the ion is of interest, therefore the electron cooling rate  $C_e$  is given by

$$C_e = n_e S_e \int_0^{\infty} \sigma_e v_e f(v_e) E_e dv_e, \quad (\text{B5})$$

where  $E_e = (1/2)m_e v_e^2$ . Substituting the known quantities into the equation gives the electron cooling rate  $C_e$  as

$$C_e = n_e S_e 4\pi^2 a^2 \left( \frac{m_e}{2\pi kT} \right)^{\frac{3}{2}} \int_0^{\infty} \left[ \left( 1 + \frac{2Ze^2}{4\pi\epsilon_0 a m_e v_e^2} \right) v^3 e^{\frac{-m_e v_e^2}{2kT}} \right] \frac{1}{2} m_e v_e^2 dv_e. \quad (\text{B6})$$

Making the substitution  $x = \frac{m_e v_e^2}{2kT}$  and integrating,  $C_e$  for positive grains is

$$C_e = n_e S_e \pi a^2 \left[ \frac{(2kT)^3}{\pi m_e} \right]^{\frac{1}{2}} \left( 2 + \frac{Ze^2}{4\pi\epsilon_0 a kT} \right). \quad (\text{B7})$$

For positive grains the electron cooling rate increases linearly with  $Z$  due to Coulomb attraction. It can be concluded from Equation B7 that the particle cooling rate should increase in a linear fashion with  $Z$  when the particle and the grain have an opposite charge state. Therefore the ion cooling rate  $C_i$  for negative grains ( $Z < 0$ ) is

$$C_i = n_i S_i \pi a^2 \left[ \frac{(2kT)^3}{\pi m_i} \right]^{\frac{1}{2}} \left( 2 - \frac{Ze^2}{4\pi\epsilon_0 a kT} \right). \quad (\text{B8})$$

# APPENDIX C

## JHPEBOX.FOR

\* This program calculates the Photoelectron Emission from Graphite  
\* dust grains. The P.E. energy distribution is box like.

\*  
DOUBLE PRECISION QY(31), LAMBDA(31)

\* QY is Q\_ABS\*Y, Lambda is photon wavelength

\*  
DOUBLE PRECISION DNDT, HPE, FUNCC1, FUNCC2, FUNC11, FUNC12,  
FUNC21, FUNC22, A, ENG1, ENG2, F1, F2, H, C, PI, C1, INTGD1, INTGD2,  
LWF, U, PB, LAMBDA, ENGX

\* DNDT is photoelectron rate, HPE is the photoelectron heating rate,  
\* FUNCC1 is inside dndt int, FUNCC2 is inside hpe int, FUNC11 & FUNC12  
\* & FUNC21 & FUNC22 are int functions, A is grain radius, ENG1 & ENG2  
\* are energies, F1 & F2 are interstellar UV, H is Planck's Const, C is  
\* speed of light in a vacuum, PI is PI, C1 is a const, INTGD1 is the  
\* integrand for dndt, INTGD2 is the integrand for hpe, WF is the work  
\* function, U is the surface potential, PB is total potential barrier,  
\* LAMBDA & ENGX are 0 cut-off values

\*  
INTEGER I, J, Z, NUMRAD, NUMWAVE, TESTER

\* I & J are counters, Z is grain charge, NUMRAD is the # of differing  
\* grain radii, NUMWAVE is the # of differing wavelengths, TESTER is a  
\* TRUE/FALSE flag

\*  
\* Initializing wavelength (LAMBDA) array

DATA(LAMBDA(I),I=1,31)/911.8,920.,940.,960.,980.,1000.,1020.,1040.

L,1060.,1080.,1100.,1120.,1140.,1160.,1180.,1200.,1220.,1240.,1260.

L,1280.,1300.,1320.,1340.,1360.,1380.,1400.,1420.,1440.,1460.,1480.

L,1500./

\*  
\* Initializing constants

H=4.136E-15

C=2.998E10

PI=3.1416

E=1.602E-19

EPSILON=8.85E-12

WF=8.

NUMRAD=15

NUMWAVE=31

```

* Files
OPEN(5,FILE='QY-GR2.DAT',STATUS='OLD')
OPEN(6,FILE='JHPEBOX.DAT',STATUS='UNKNOWN')
*
* Writing header
WRITE(*,6)
WRITE(6,6)
WRITE(*,7)
WRITE(6,7)
*
* Reading input data
J=1
DOWHILE(J.LE.NUMRAD)
  READ(5,*) A
  I=1
  DOWHILE(I.LE.NUMWAVE)
    READ(5,*) QY(I)
    I=I+1
  ENDDO
*
* Calculating HPE for negative Z
C1=(4.*(PI**2)*(1.E-8)*H*C*(A**2))
Z=-30
U=Z*E*(1.E10)*(6.242E18)/(4*PI*EPSILON*A)
DNDT=0.
HPE=0.
DOWHILE(Z.LT.0)
  I=1
  INTGD2=0.
  FUNCC2=0.
  DOWHILE(I.LE.(NUMWAVE-1))
    INTGD2=INTGD2+FUNCC2
    ENG1=((1.0E8)*H*C)/LAMBDA(I)
    ENG2=((1.0E8)*H*C)/LAMBDA(I+1)
    F1=(1.658E6*ENG1)-(2.152E5*ENG1**2.)+(6.919E3*ENG1**3.)
    F2=(1.658E6*ENG2)-(2.152E5*ENG2**2.)+(6.919E3*ENG2**3.)
    FUNC21=(1./(LAMBDA(I)**2.))*F1*QY(I)*(0.5*(ENG1-WF)-E*U)
    FUNC22=(1./(LAMBDA(I+1)**2.))*F2*QY(I+1)*(0.5*(ENG2-WF)-E
L   *U)
    FUNCC2=(0.5)*(FUNC21+FUNC22)*(LAMBDA(I+1)-LAMBDA(I))
    I=I+1
  ENDDO
  HPE=C1*(INTGD2+FUNCC2)
  WRITE(*,10) A,Z,DNDT,HPE
  WRITE(6,10) A,Z,DNDT,HPE

```



```

Z=Z+1
U=Z*E*(1.E10)*(6.242E18)/(4*PI*EPSILON*A)
ENDDO
*
* Calculating DNDT (Photoelectron Rate {P.E.})
Z=0
U=0
PB=WF+E*U
TESTER=0
DNDT=0
* Begin if the most energetic photon can produce a P.E.
DOWHILE(((H*C*(1.0E8)/LAMBDA(1))-PB).GE.0)
I=1
INTGD1=0.
INTGD2=0.
FUNCC1=0.
FUNCC2=0.
* Do for all wavelengths or until energy will not produce a P.E.
DOWHILE((I.LE.(NUMWAVE-1)).AND.(TESTER.NE.1))
INTGD1=INTGD1+FUNCC1
INTGD2=INTGD2+FUNCC2
ENG1=((1.0E8)*H*C)/LAMBDA(I)
ENG2=((1.0E8)*H*C)/LAMBDA(I+1)
* Do if the energy of the first photon can produce a P.E.
IF((ENG1-PB).GT.0)THEN
F1=(1.658E6*ENG1)-(2.152E5*ENG1**2.)+(6.919E3*ENG1
L **3.)
FUNC11=(1./(LAMBDA(I)**2.))*F1*QY(I)*((ENG1-PB)/(ENG1-
L WF))
FUNC21=(1./(LAMBDA(I)**2.))*F1*QY(I)*(0.5*((ENG1-PB)**
L 2/(ENG1-WF)))
* Do if the energy of the second photon can produce a P.E.
IF((ENG2-PB).GT.0)THEN
F2=(1.658E6*ENG2)-(2.152E5*ENG2**2.)+(6.919E3*ENG2
L **3.)
FUNC12=(1./(LAMBDA(I+1)**2.))*F2*QY(I+1)*((ENG2-PB)
L /(ENG2-WF))
FUNC22=(1./(LAMBDA(I+1)**2.))*F2*QY(I+1)*(0.5*((
L ENG2-PB)**2/(ENG2-WF)))
FUNCC1=(0.5)*(FUNC11+FUNC12)*(LAMBDA(I+1)-LAMBDA(I)
L )
FUNCC2=(0.5)*(FUNC21+FUNC22)*(LAMBDA(I+1)-LAMBDA(I)
L )
* If the second photon's energy is less than the barrier and the first
* photon's is not, then a cut-off wavelength is calculated & the func2

```

```

*      is set to 0 at that energy.
      ELSE
        ENGX=PB
        LAMBDA X=H*C*(1.E8)/ENGX
        FUNC12=0
        FUNC22=0
        FUNCC1=(0.5)*(FUNC11+FUNC12)*(LAMBDA X-LAMBDA(I))
        FUNCC2=(0.5)*(FUNC21+FUNC22)*(LAMBDA X-LAMBDA(I))
*      Now it is no longer necessary to continue with the next wavelength
*      because the are in decending energy order.
        TESTER=1
      END IF
    ELSE
*      Now it is no longer necessary to continue with the next wavelength
*      because the are in decending energy order.
        TESTER=1
      END IF
*      Incrementing wavelength
      I=I+1
    ENDDO
    DNDT=C1*(INTGD1+FUNCC1)
    HPE=C1*(INTGD2+FUNCC2)
    WRITE(*,10) A,Z,DNDT,HPE
    WRITE(6,10) A,Z,DNDT,HPE
*      Intializing for next charge increment
      Z=Z+1
      U=Z*E*(1.E10)*(6.242E18)/(4*PI*EPSILON*A)
      PB=WF+E*U
      TESTER=0
    ENDDO
    WRITE(*,*)
    WRITE(6,*)
*      Incrementing radius
      J=J+1
    ENDDO
*
*      Formats
    6 FORMAT(/3X,'GRAIN RAD.(A)',3X,'CHARGE',5X,'DNDT (1/SEC)',6X,
      L'HPE (E/SEC)')
    7 FORMAT(3X,'-----',3X,'-----',5X,'-----',
      L5X,'-----'/)
    10 FORMAT(4X,F8.1,2X,I8,7X,E12.6,5X,E12.6)

    STOP
    END

```

# APPENDIX D

## JHPETENT.FOR

```
* This program calculates the Photoelectron Emission from Graphite
* dust grains. The P.E. energy distribution is tent like.
*
DOUBLE PRECISION QY(31), LAMBDA(31)
* QY is Q_ABS*Y, Lambda is photon wavelength
*
DOUBLE PRECISION DNDT, HPE, FUNCC1, FUNCC2, FUNC11, FUNC12,
LFUNC21, FUNC22, A, ENG1, ENG2, F1, F2, H, C, PI, C1, INTGD1, INTGD2,
LWF, U, PB, LAMBDA_X, ENG_X
* DNDT is photoelectron rate, HPE is the photoelectron heating rate,
* FUNCC1 is inside dndt int, FUNCC2 is inside hpe int, FUNC11 & FUNC12
* & FUNC21 & FUNC22 are int functions, A is grain radius, ENG1 & ENG2
* are energies, F1 & F2 are interstellar UV, H is Planck's Const, C is
* speed of light in a vacuum, PI is PI, C1 is a const, INTGD1 is the
* integrand for dndt, INTGD2 is the integrand for hpe, WF is the work
* function, U is the surface potential, PB is total potential barrier,
* LAMBDA_X & ENG_X are 0 cut-off values
*
INTEGER I, J, Z, NUMRAD, NUMWAVE, TESTER
* I & J are counters, Z is grain charge, NUMRAD is the # of differing
* grain radii, NUMWAVE is the # of differing wavelengths, TESTER is a
* TRUE/FALSE flag
*
* Initializing wavelength (LAMBDA) array
DATA(LAMBDA(I),I=1,31)/911.8,920.,940.,960.,980.,1000.,1020.,1040.
L,1060.,1080.,1100.,1120.,1140.,1160.,1180.,1200.,1220.,1240.,1260.
L,1280.,1300.,1320.,1340.,1360.,1380.,1400.,1420.,1440.,1460.,1480.
L,1500./
*
* Initializing constants
H=4.136E-15
C=2.998E10
PI=3.1416
E=1.602E-19
EPSILON=8.85E-12
WF=8.
NUMRAD=15
NUMWAVE=31
```

```

*
* Files
OPEN(5,FILE='QY-GR2.DAT',STATUS='OLD')
OPEN(6,FILE='JHPETENT.DAT',STATUS='UNKNOWN')
*
* Writing file header
WRITE(*,6)
WRITE(6,6)
WRITE(*,7)
WRITE(6,7)
*
* Reading input data
J=1
* Beginning the radius loop
DOWHILE(J.LE.NUMRAD)
  READ(5,*) A
  I=1
* Reading all QY data for a specific radius
  DOWHILE(I.LE.NUMWAVE)
    READ(5,*) QY(I)
    I=I+1
  ENDDO
*
* Calculating HPE for negative Z
C1=(4.*(PI**2)*(1.E-8)*H*C*(A**2))
Z=-30
U=Z*E*(1.E10)*(6.242E18)/(4*PI*EPSILON*A)
DNDDT=0.
HPE=0.
DOWHILE(Z.LT.0)
  I=1
  INTGD2=0.
  FUNCC2=0.
  DOWHILE(I.LE.(NUMWAVE-1))
    INTGD2=INTGD2+FUNCC2
    ENG1=((1.0E8)*H*C)/LAMBDA(I)
    ENG2=((1.0E8)*H*C)/LAMBDA(I+1)
    F1=(1.658E6*ENG1)-(2.152E5*ENG1**2.)+(6.919E3*ENG1**3.)
    F2=(1.658E6*ENG2)-(2.152E5*ENG2**2.)+(6.919E3*ENG2**3.)
    FUNC21=(1./(LAMBDA(I)**2.))*F1*QY(I)*(0.5*(ENG1-WF)-E*U)
    FUNC22=(1./(LAMBDA(I+1)**2.))*F2*QY(I+1)*(0.5*(ENG2-WF)-E
L    *U)
    FUNCC2=(0.5)*(FUNC21+FUNC22)*(LAMBDA(I+1)-LAMBDA(I))
    I=I+1
  ENDDO

```

```

HPE=C1*(INTGD2+FUNCC2)
WRITE(*,10) A,Z,DNDT,HPE
WRITE(6,10) A,Z,DNDT,HPE
Z=Z+1
U=Z*E*(1.E10)*(6.242E18)/(4*PI*EPSILON*A)
ENDDO
*
* Calculating DNDT (Photoelectron Rate {P.E.})
C1=(4.*(PI**2)*(1.E-8)*H*C*(A**2))
Z=0
U=0
PB=WF+E*U
TESTER=0
DNDT=0.
HPE=0.
* Begin if the most energetic photon can produce a P.E.
DOWHILE(((H*C*(1.0E8)/LAMBDA(1))-PB).GE.0)
  I=1
  INTGD1=0.
  INTGD2=0.
  FUNCC1=0.
  FUNCC2=0.
* Do for all wavelengths or until energy will not produce a P.E.
DOWHILE((I.LE.(NUMWAVE-1)).AND.(TESTER.LT.1))
  INTGD1=INTGD1+FUNCC1
  INTGD2=INTGD2+FUNCC2
  ENG1=((1.0E8)*H*C)/LAMBDA(I)
  ENG2=((1.0E8)*H*C)/LAMBDA(I+1)
* Do if the energy of the first photon can produce a P.E.
IF((ENG1-PB).GT.0)THEN
  F1=(1.658E6*ENG1)-(2.152E5*ENG1**2.)+(6.919E3*ENG1
L   **3.)
* If the tent midpoint is >0 then entire tent function
IF((0.5*(ENG1-WF))-E*U.GT.0)THEN
  FUNC11=(1./(LAMBDA(I)**2.))*F1*QY(I)*(1-(2*(E*U)**2
L   )/(ENG1-WF)**2)
  FUNC21=(1./(LAMBDA(I)**2.))*F1*QY(I)*(((4*(E*U)**3)
L   +(3*(ENG1-WF)**3)-(6*E*U*(ENG1-WF)**2))/(6*(ENG1-
L   WF)**2))
* Or just half the tent function
ELSE
  FUNC11=(1./(LAMBDA(I)**2.))*F1*QY(I)*(2*((ENG1-PB)*
L   *2)/(ENG1-WF)**2)
  FUNC21=(1./(LAMBDA(I)**2.))*F1*QY(I)*((2*(ENG1-PB)*
L   *3)/(3*(ENG1-WF)**2))

```

```

END IF
* Do if the energy of the second photon can produce a P.E.
IF((ENG2-PB).GT.0)THEN
  F2=(1.658E6*ENG2)-(2.152E5*ENG2**2.)+(6.919E3*ENG2*
L   *3.)
* If the tent midpoint is >0 then entire tent function
IF((0.5*(ENG2-WF))-E*U.GT.0)THEN
  FUNC12=(1./(LAMBDA(I+1)**2.))*F2*QY(I+1)*(1-(2*(
L   E*U)**2)/(ENG2-WF)**2)
  FUNC22=(1./(LAMBDA(I+1)**2.))*F2*QY(I+1)*(((4*(E
L   *U)**3)+(3*(ENG2-WF)**3)-(6*E*U*(ENG2-WF)**2))/
L   (6*(ENG2-WF)**2))
  FUNCC1=(0.5)*(FUNC11+FUNC12)*(LAMBDA(I+1)-LAMBDA
L   (I))
  FUNCC2=(0.5)*(FUNC21+FUNC22)*(LAMBDA(I+1)-LAMBDA
L   (I))
* Or just half the tent fuction
ELSE
  FUNC12=(1./(LAMBDA(I+1)**2.))*F2*QY(I+1)*(2*((EN
L   G2-PB)**2)/(ENG2-WF)**2)
  FUNC22=(1./(LAMBDA(I+1)**2.))*F2*QY(I+1)*((2*(EN
L   G2-PB)**3)/(3*(ENG2-WF)**2))
  FUNCC1=(0.5)*(FUNC11+FUNC12)*(LAMBDA(I+1)-LAMBDA
L   (I))
  FUNCC2=(0.5)*(FUNC21+FUNC22)*(LAMBDA(I+1)-LAMBDA
L   (I))
  END IF
* If the second photon's energy is less than the barrier and the first
* photon's is not, then a cut-off wavelength is calculated & the func2
* is set to 0 at that energy.
ELSE
  ENGX=PB
  LAMBDA X=H*C*(1.E8)/ENGX
  FUNC12=0
  FUNC22=0
  FUNCC1=(0.5)*(FUNC11+FUNC12)*(LAMBDA X-LAMBDA(I))
  FUNCC2=(0.5)*(FUNC21+FUNC22)*(LAMBDA X-LAMBDA(I))
* Now it is no longer necessary to continue with the next wavelength
* because the are in decending energy order.
  TESTER=1
  END IF
ELSE
* Now it is no longer necessary to continue with the next wavelength
* because the are in decending energy order.
  TESTER=1

```

```

        END IF
*       Incrementing wavelength
        I=I+1
        ENDDO
        DNDT=C1*(INTGD1+FUNCC1)
        HPE=C1*(INTGD2+FUNCC2)
        WRITE(*,10) A,Z,DNDT,HPE
        WRITE(6,10) A,Z,DNDT,HPE
*       Intializing for next charge increment
        Z=Z+1
        U=Z*E*(1.E10)*(6.242E18)/(4*PI*EPSILON*A)
        PB=WF+E*U
        TESTER=0
        ENDDO
        WRITE(*,*)
        WRITE(6,*)
*       Incrementing radius
        J=J+1
        ENDDO
*
*       Formats
6 FORMAT(/3X,'GRAIN RAD.(A)',3X,'CHARGE',5X,'DNDT (1/SEC)',6X,
L'HPE (E/SEC)')
7 FORMAT(3X,'-----',3X,'-----',5X,'-----',
L5X,'-----'/)
10 FORMAT(4X,F8.1,2X,I8,7X,E12.6,5X,E12.6)

        STOP
        END

```

# **APPENDIX E**

## **Figures**



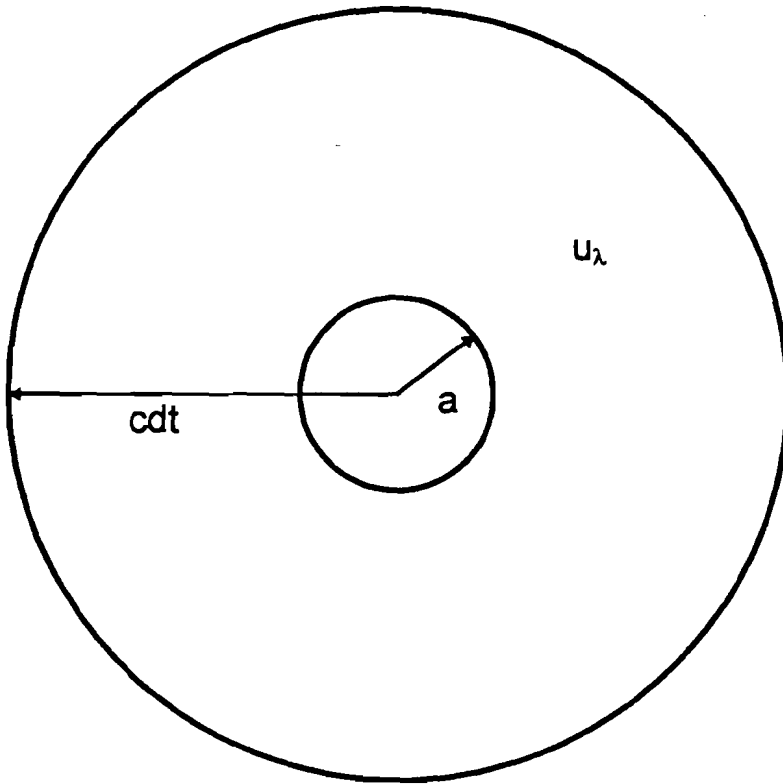


Figure 1. A grain of radius  $a$  immersed in an isotropic photon field of energy density  $u_\lambda$ . All photons which are absorbed in time  $dt$  must be within a spherical volume of radius  $cdt$ .

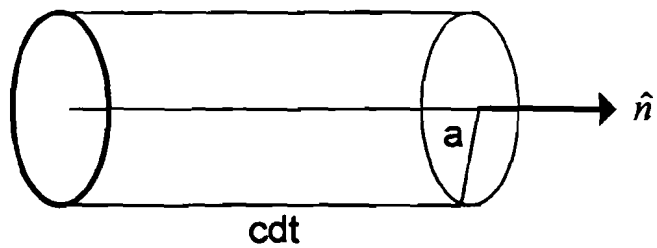


Figure 2. Photons within the cylindrical region and having direction  $-\hat{n}$  will be absorbed by the grain.

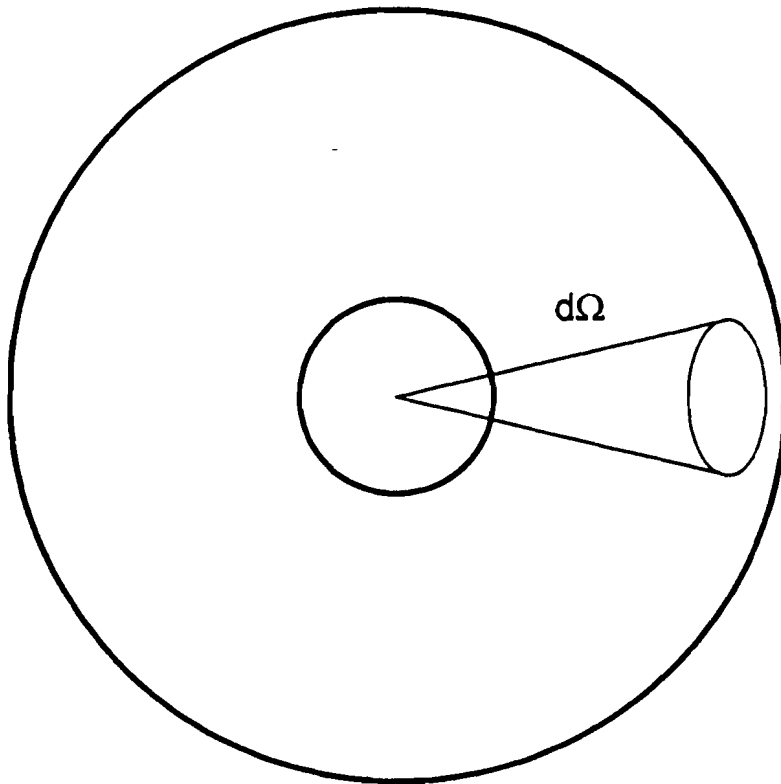


Figure 3. Absorbed photons' directions are defined by a **differential** element of solid angle  $d\Omega$  which is centered about the cylindrical region in Figure 2.

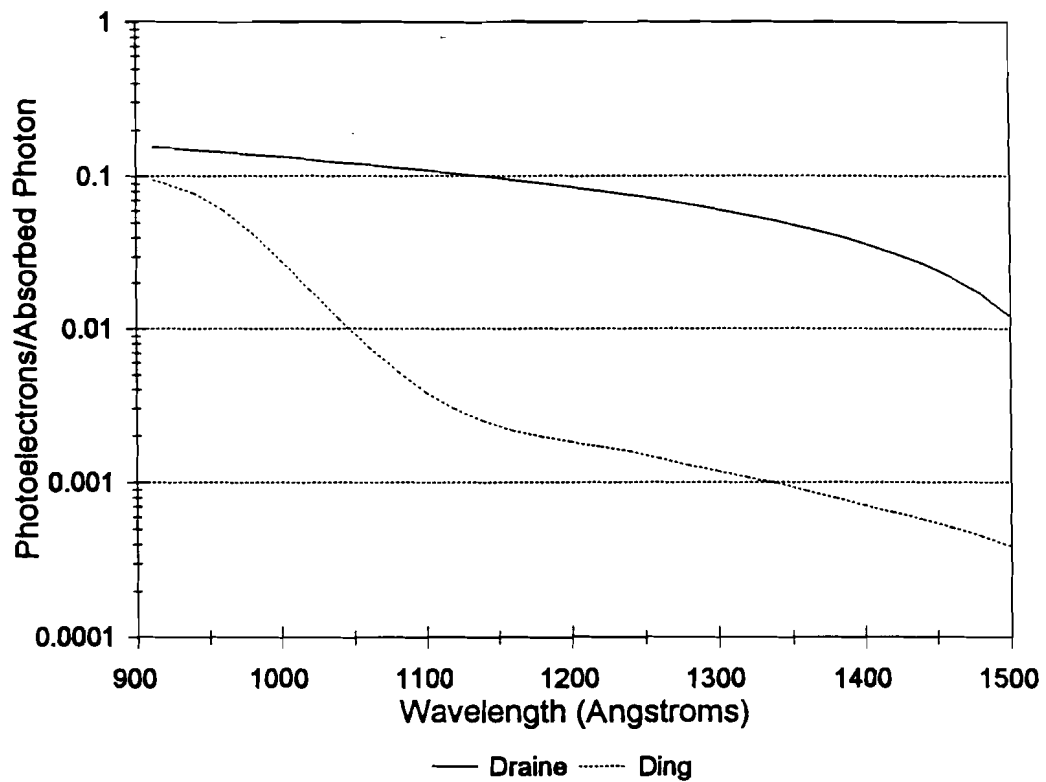


Figure 4. Photon absorption efficiency  $Q$  times photoelectric yield  $Y$  plotted as a function of photon wavelength, for  $100 \text{ \AA}$  graphite grains. The solid curve represents Draine's<sup>6</sup> assumed function and the dotted curve represents Ding's<sup>5</sup> calculations.

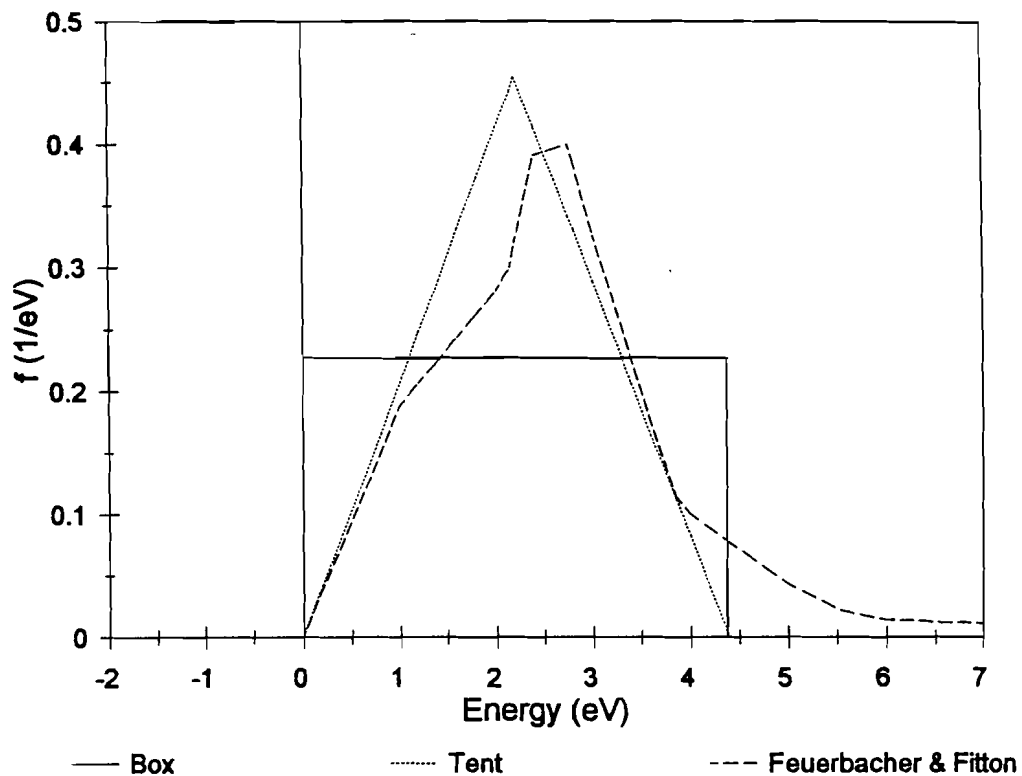


Figure 5. Normalized photoelectron kinetic energy spectra of graphite. The dashed curve represents the experimental results of Feuerbacher and Fitton<sup>14</sup> for 12.4 eV photons incident on bulk graphite. The solid curve represents the corresponding box spectrum of Draine<sup>6</sup> and the dotted curve represents the corresponding tent spectrum.

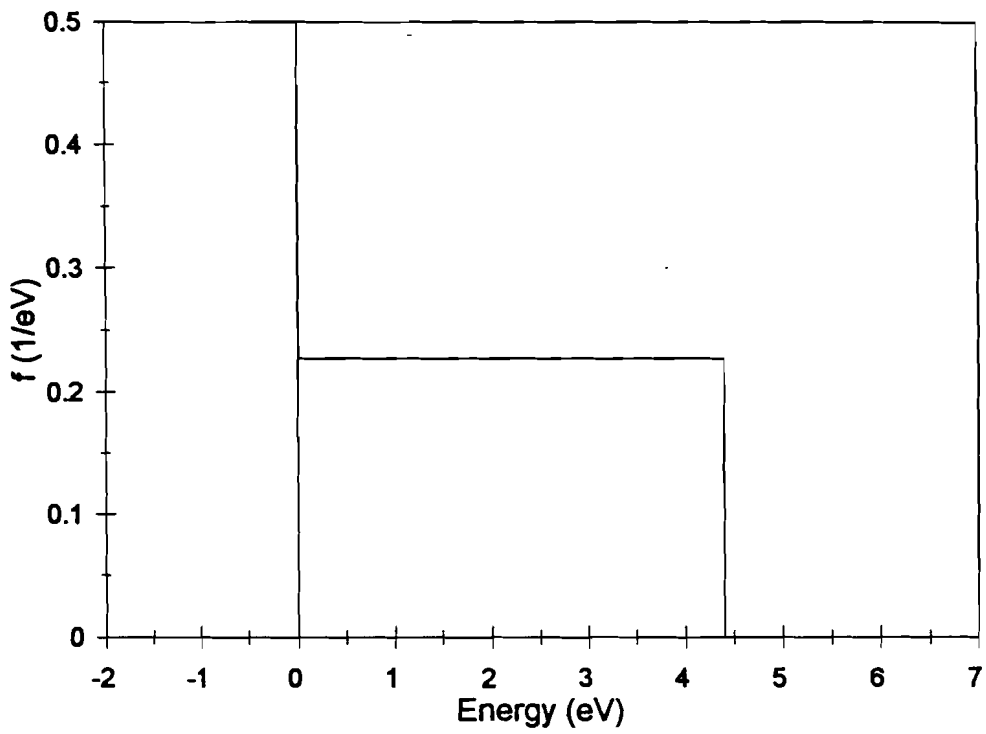


Figure 6. The normalized box photoelectron kinetic energy spectrum of a neutral graphite grain.

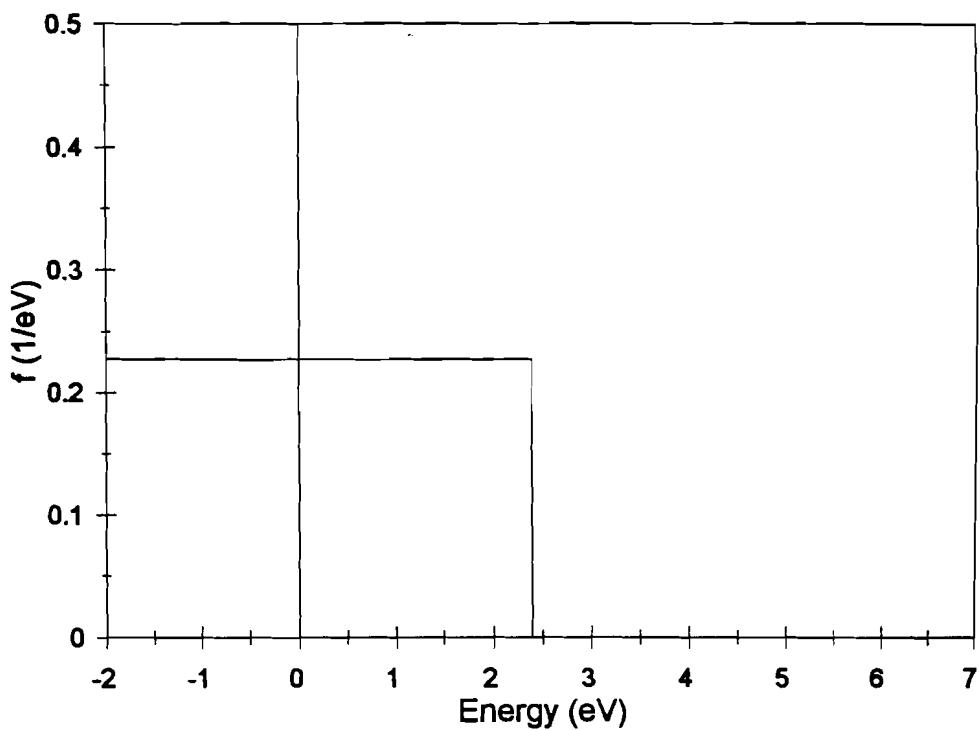


Figure 7. The normalized box photoelectron kinetic energy spectrum of a positively charged graphite grain. In this example, the surface potential is 2 V. The portion of the distribution below 0 represents electrons with insufficient energy to escape from the surface potential.

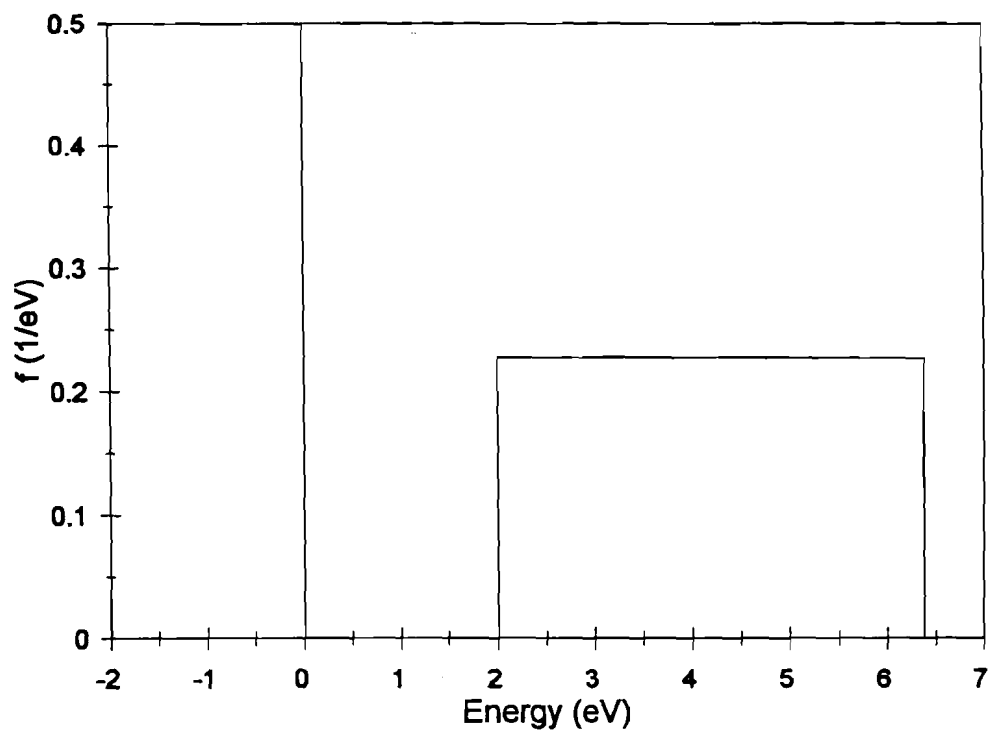


Figure 8. The normalized box photoelectron kinetic energy spectrum of a negative graphite grain. In this example, the surface potential is  $-2$  V.



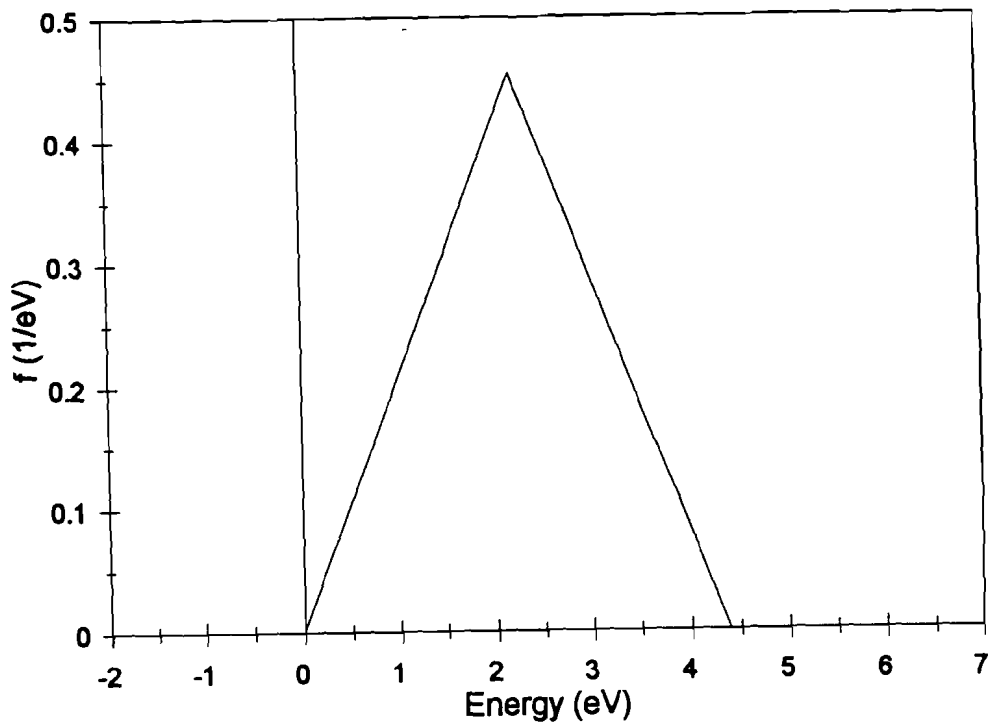


Figure 9. The normalized tent photoelectron kinetic energy spectrum of a neutral graphite grain.

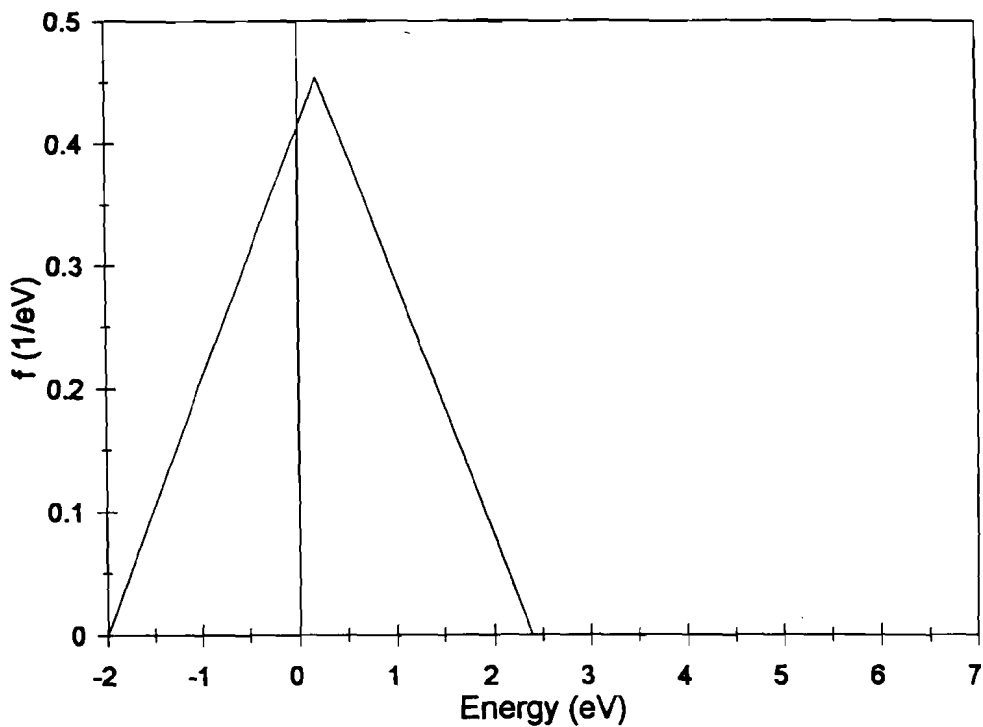


Figure 10. The normalized tent photoelectron kinetic energy spectrum of a positively charged graphite grain. In this example, the surface potential is 2 V. The portion of the distribution below 0 represents electrons with insufficient energy to escape from the surface potential.

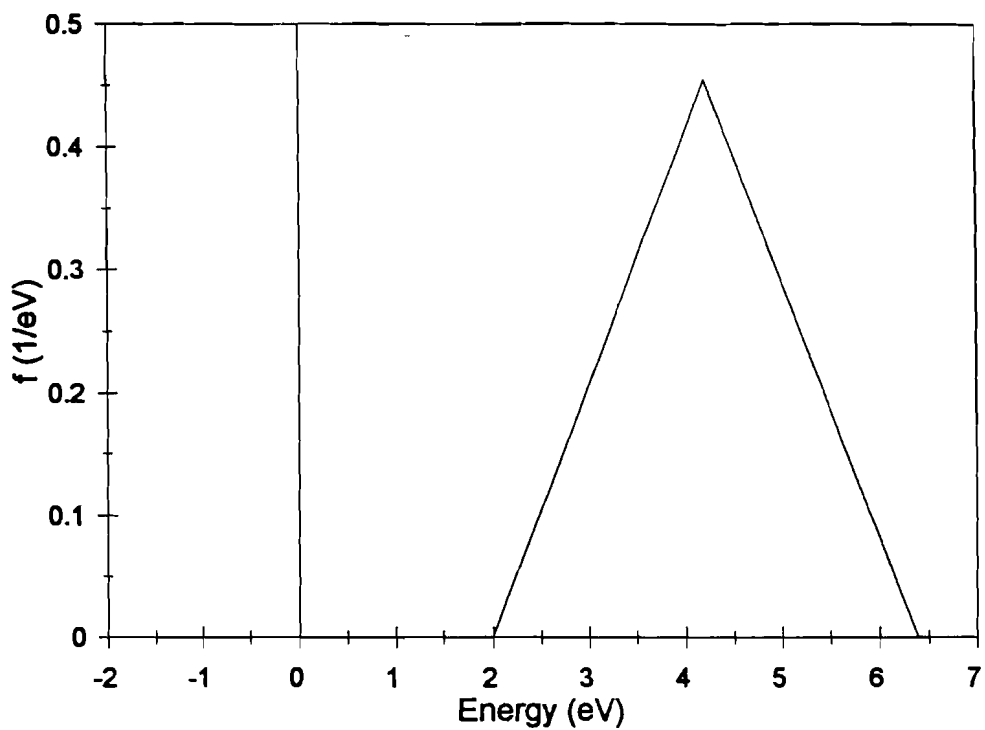


Figure 11. The normalized tent photoelectron kinetic energy spectrum of a negative graphite grain. In this example, the surface potential is  $-2$  V.

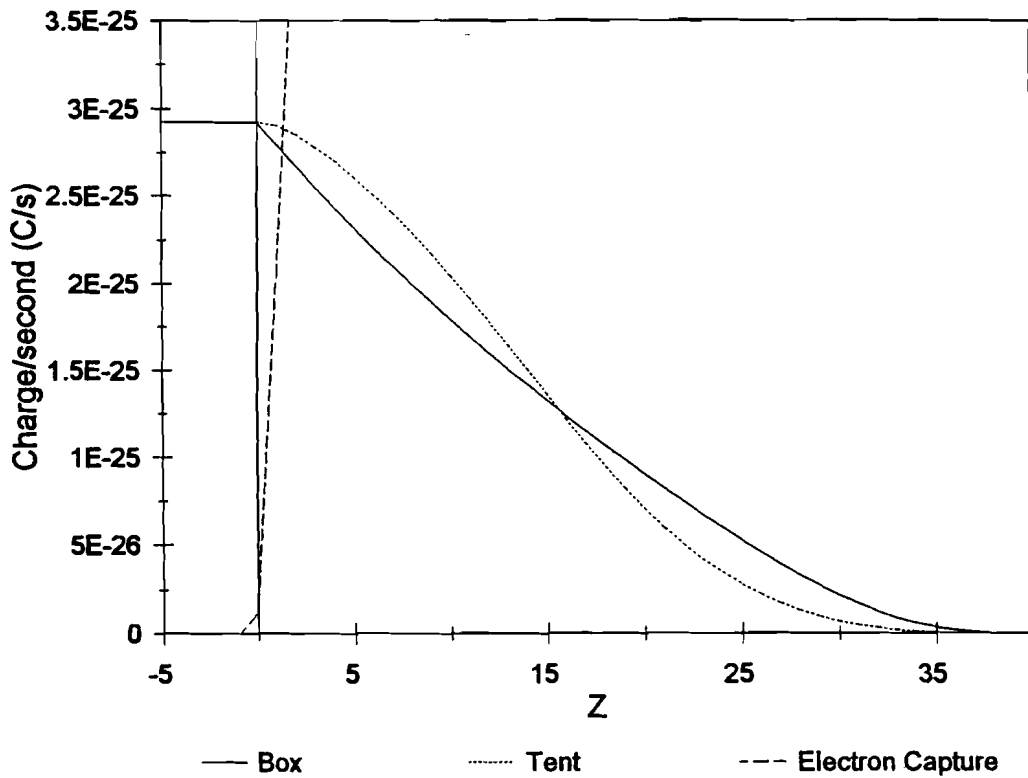


Figure 12. Photoemission rate  $J_{pe}$  and electron capture rate  $J_e$  plotted as a function of grain charge, for  $100 \text{ \AA}$  graphite grains. The solid curve represents  $J_{pe}$  calculated using the box function and the dotted curve represents  $J_{pe}$  calculated using the tent function. The dashed curve represents  $J_e$  for a grain located in a cool atomic cloud.

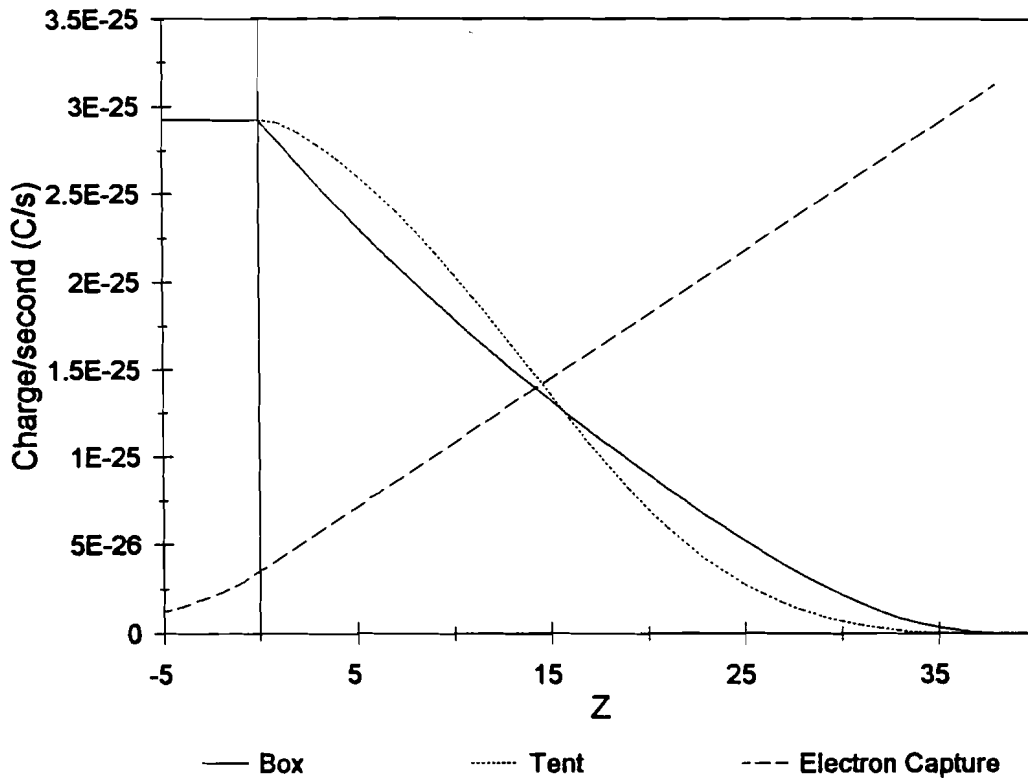


Figure 13. Photoemission rate  $J_{pe}$  and electron capture rate  $J_e$  plotted as a function of grain charge, for  $100 \text{ \AA}$  graphite grains. The solid curve represents  $J_{pe}$  calculated using the box function and the dotted curve represents  $J_{pe}$  calculated using the tent function. The dashed curve represents  $J_e$  for a grain located in a warm intercloud medium.

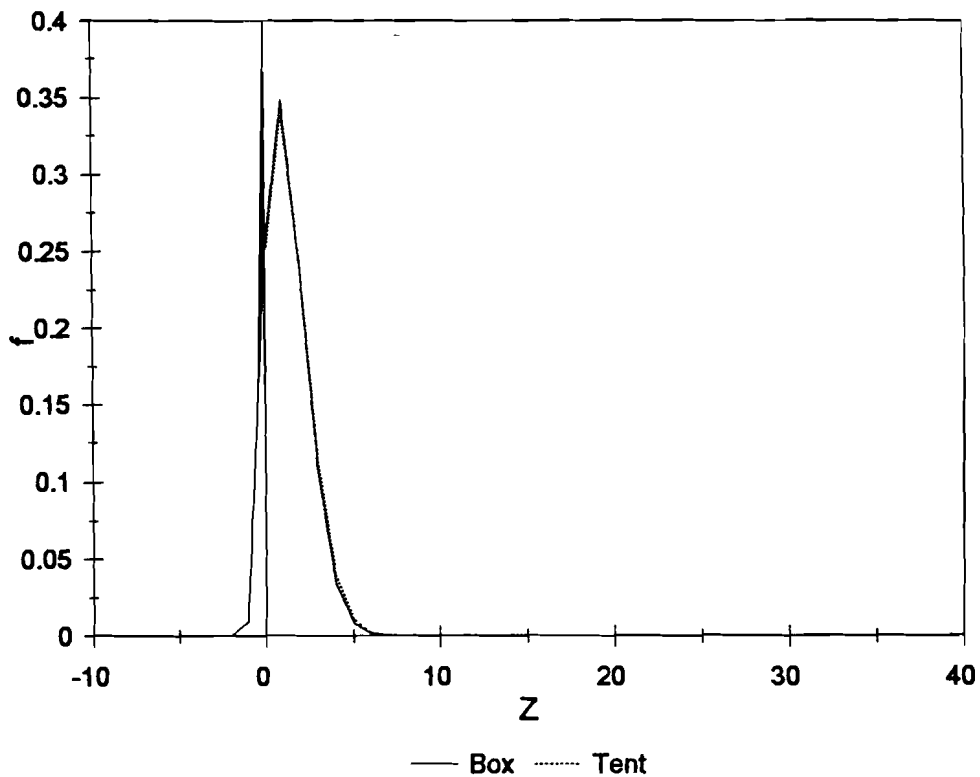


Figure 14. Charge probability distributions for 100 Å graphite grains located in a cool atomic cloud. The solid curve represents the charge probability distribution calculated using the box function and the dotted curve represents the charge probability distribution calculated using the tent function.

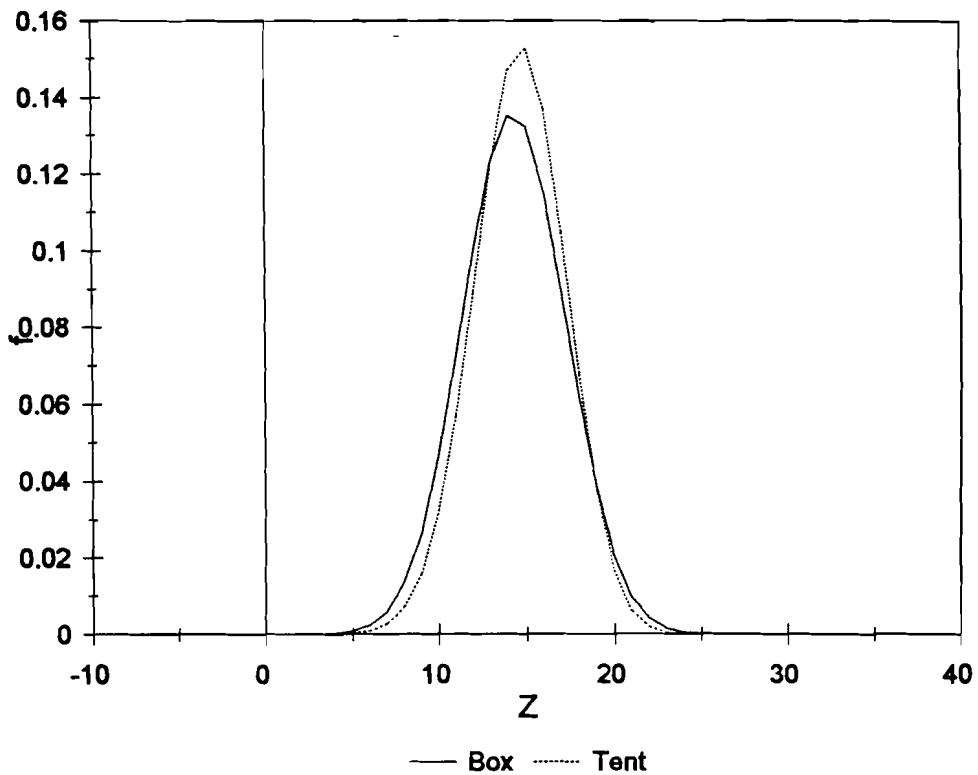


Figure 15. Charge probability distributions for 100 Å graphite grains located in a warm intercloud medium. The solid curve represents the charge probability distribution calculated using the box function and the dotted curve represents the charge probability distribution calculated using the tent function.

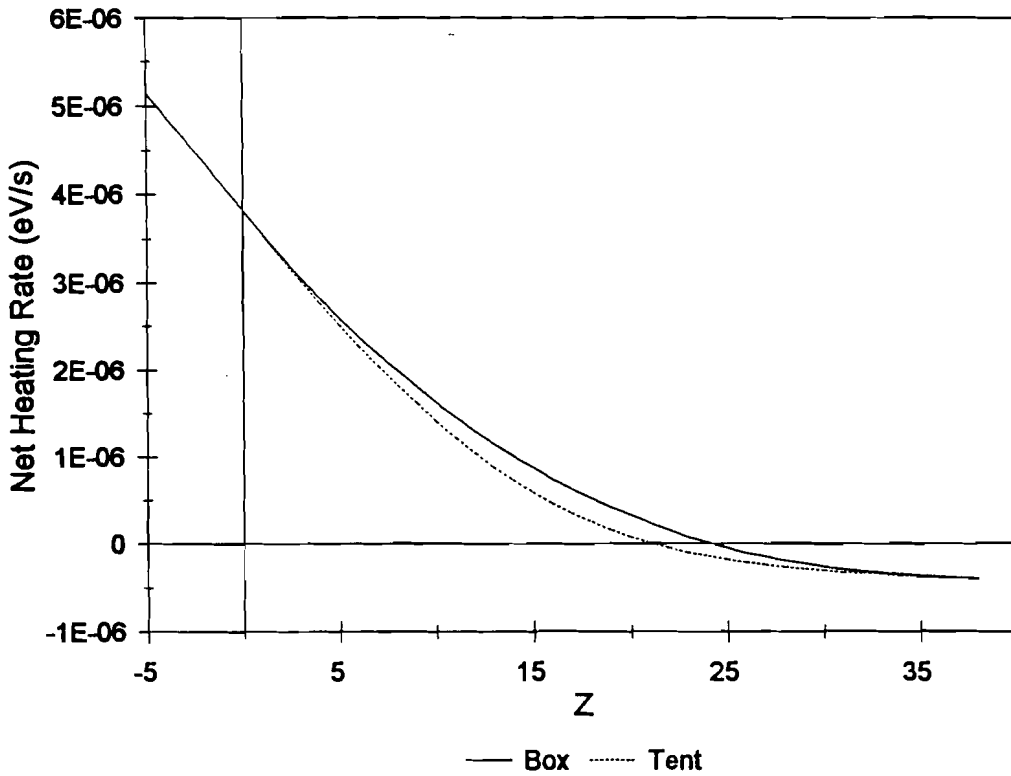


Figure 16. Net heating rates  $H_{pe} - C_e$  plotted as a function of grain charge, for  $100 \text{ \AA}$  graphite grains in a cool atomic cloud. The solid curve represents the net heating rate calculated using the box function and the dotted curve represents the net heating rate calculated using the tent function.



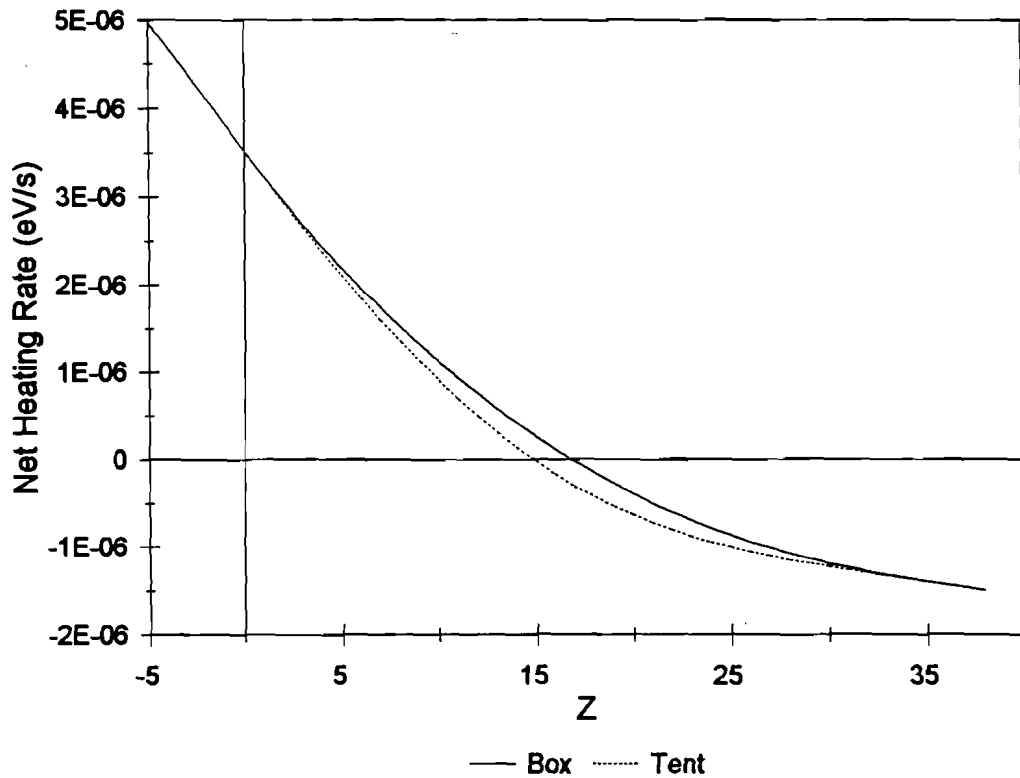


Figure 17. Net heating rates  $H_{pe} - C_e$  plotted as a function of grain charge, for  $100 \text{ \AA}$  graphite grains in a warm intercloud medium. The solid curve represents the net heating rate calculated using the box function and the dotted curve represents the net heating rate calculated using the tent function.

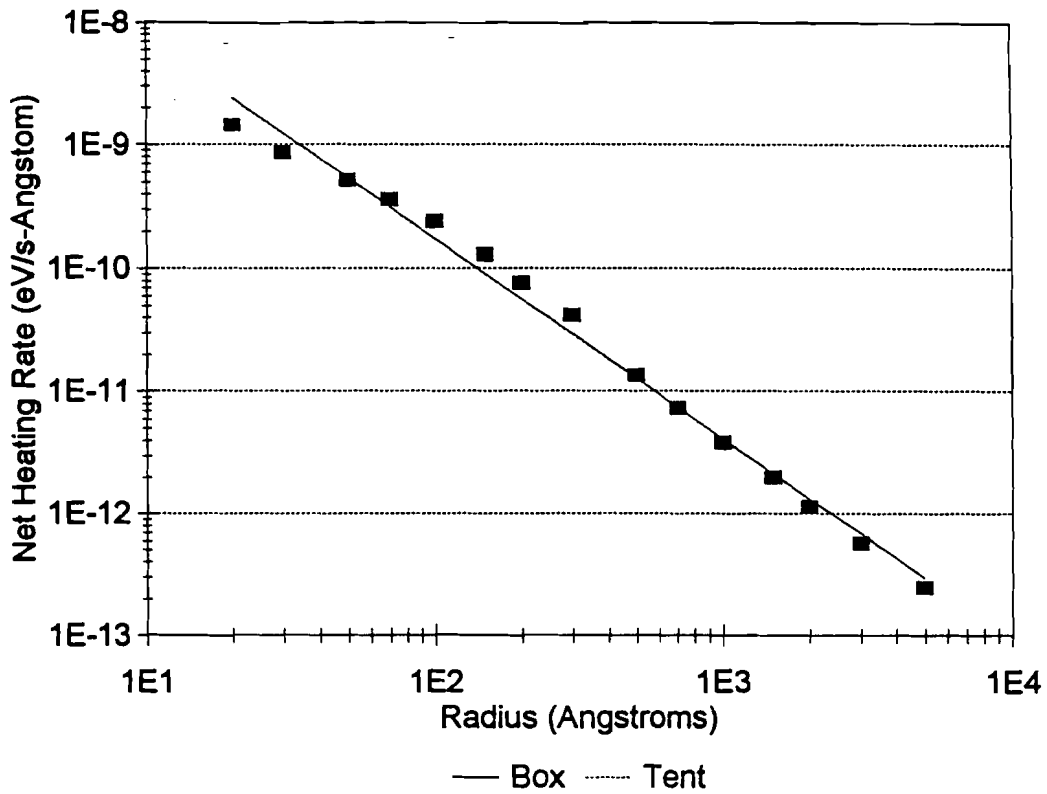


Figure 18. Net heating per grain radius interval  $H_{pe} - C_e$  plotted as a function of grain radius for graphite grains located in a cool atomic cloud. The solid boxes represent points calculated using the box function and the solid line represents the power law best fit to these points. Although points calculated using the tent function are included, the differences between the box and tent function calculations are not discernible in this graph.

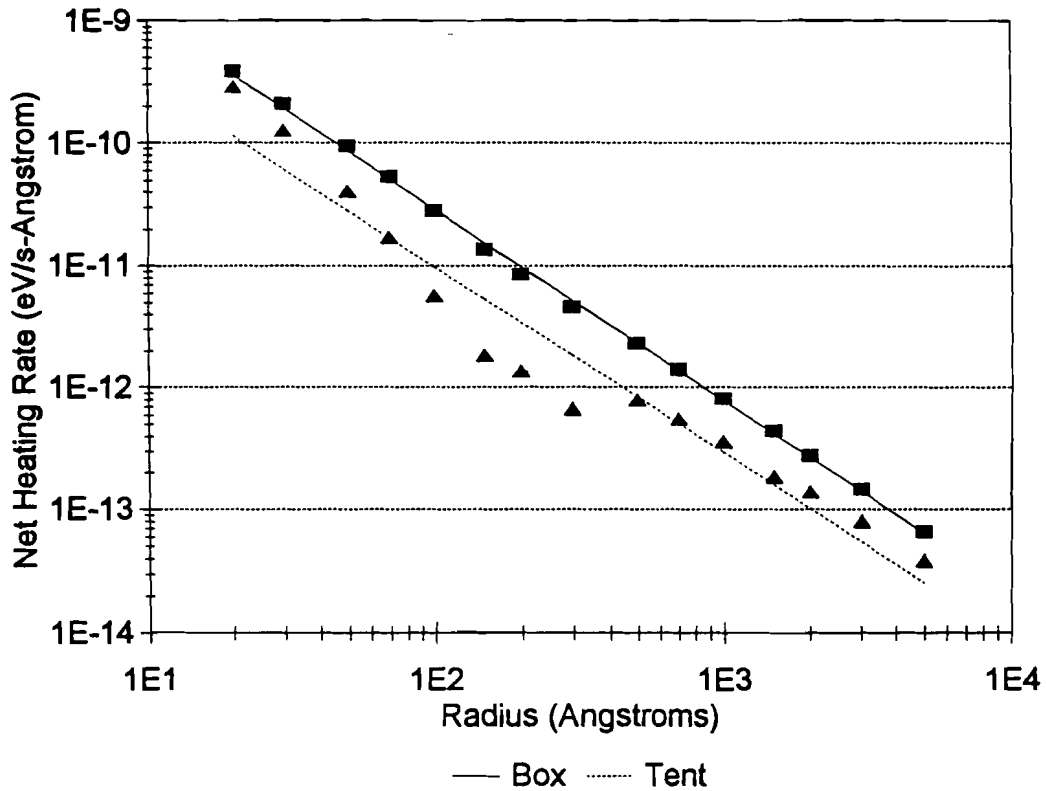


Figure 19. Net heating per grain radius interval  $H_{pe} - C_e$  plotted as a function of grain radius for graphite grains located in a warm intercloud medium. The solid boxes represent points calculated using the box function and the solid line represents the power law best fit to these points. The solid triangles represent points calculated using the tent function and the dotted line represents the power law best fit to these points.

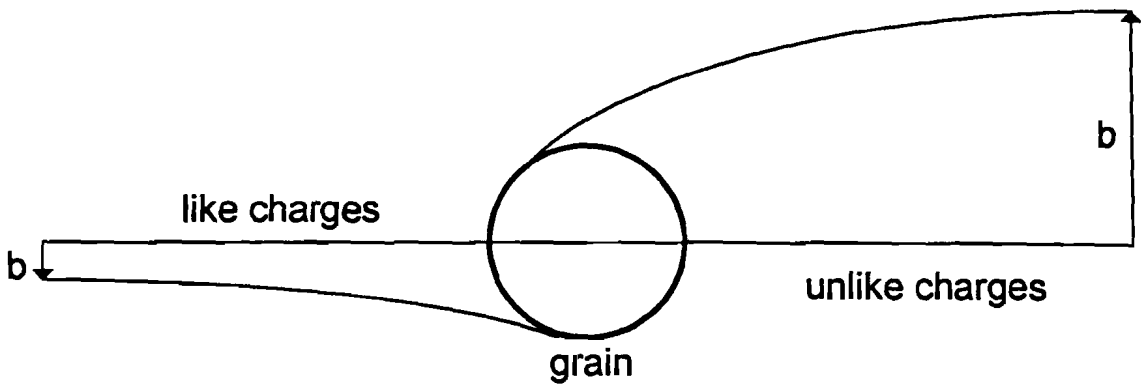


Figure 20. A grazing collision between a charged particle and a charged dust grain. The left-hand side depicts a collision where the particle and grain have like charge states. The right-hand side is a collision where the particle and grain have unlike charge states. The impact parameter  $b$  is shown for each case.

# **APPENDIX F**

## **Tables**

Angstroms  $\lambda$   
a

|       | 20       | 30       | 50       | 70       | 100      | 150      | 200      | 300      |
|-------|----------|----------|----------|----------|----------|----------|----------|----------|
| 911.8 | 0.047354 | 0.060790 | 0.079286 | 0.090599 | 0.094244 | 0.076735 | 0.065729 | 0.065729 |
| 920   | 0.044070 | 0.056620 | 0.074116 | 0.085301 | 0.090132 | 0.074660 | 0.063773 | 0.063773 |
| 940   | 0.035592 | 0.045789 | 0.060352 | 0.070522 | 0.077349 | 0.067344 | 0.057252 | 0.057252 |
| 960   | 0.026588 | 0.034224 | 0.045284 | 0.053477 | 0.060567 | 0.055819 | 0.047476 | 0.047476 |
| 980   | 0.018115 | 0.023320 | 0.030920 | 0.036778 | 0.042761 | 0.041818 | 0.035837 | 0.035837 |
| 1000  | 0.011599 | 0.014934 | 0.019837 | 0.023739 | 0.028237 | 0.029304 | 0.025500 | 0.025500 |
| 1020  | 0.007216 | 0.009296 | 0.012380 | 0.014912 | 0.018125 | 0.019953 | 0.017769 | 0.017769 |
| 1040  | 0.004494 | 0.005793 | 0.007738 | 0.009381 | 0.011629 | 0.013558 | 0.012465 | 0.012465 |
| 1060  | 0.002884 | 0.003720 | 0.004982 | 0.006072 | 0.007650 | 0.009403 | 0.009006 | 0.009006 |
| 1080  | 0.001953 | 0.002520 | 0.003378 | 0.004130 | 0.005260 | 0.006756 | 0.006797 | 0.006797 |
| 1100  | 0.001419 | 0.001830 | 0.002450 | 0.002994 | 0.003828 | 0.005062 | 0.005370 | 0.005370 |
| 1120  | 0.001119 | 0.001441 | 0.001922 | 0.002338 | 0.002977 | 0.003981 | 0.004420 | 0.004420 |
| 1140  | 0.000950 | 0.001221 | 0.001620 | 0.001956 | 0.002466 | 0.003299 | 0.003756 | 0.003756 |
| 1160  | 0.000856 | 0.001098 | 0.001447 | 0.001733 | 0.002157 | 0.002879 | 0.003297 | 0.003297 |
| 1180  | 0.000802 | 0.001027 | 0.001345 | 0.001597 | 0.001962 | 0.002613 | 0.003015 | 0.003015 |
| 1200  | 0.000763 | 0.000975 | 0.001271 | 0.001499 | 0.001818 | 0.002406 | 0.002873 | 0.002873 |
| 1220  | 0.000725 | 0.000925 | 0.001200 | 0.001407 | 0.001688 | 0.002203 | 0.002756 | 0.002756 |
| 1240  | 0.000681 | 0.000868 | 0.001122 | 0.001309 | 0.001557 | 0.001993 | 0.002545 | 0.002545 |
| 1260  | 0.000630 | 0.000802 | 0.001034 | 0.001202 | 0.001418 | 0.001781 | 0.002245 | 0.002245 |
| 1280  | 0.000579 | 0.000737 | 0.000947 | 0.001097 | 0.001285 | 0.001587 | 0.001946 | 0.001946 |
| 1300  | 0.000534 | 0.000679 | 0.000871 | 0.001005 | 0.001170 | 0.001424 | 0.001701 | 0.001701 |
| 1320  | 0.000495 | 0.000628 | 0.000804 | 0.000925 | 0.001071 | 0.001287 | 0.001507 | 0.001507 |
| 1340  | 0.000456 | 0.000579 | 0.000740 | 0.000849 | 0.000977 | 0.001161 | 0.001339 | 0.001339 |
| 1360  | 0.000416 | 0.000528 | 0.000673 | 0.000770 | 0.000882 | 0.001037 | 0.001180 | 0.001180 |
| 1380  | 0.000376 | 0.000476 | 0.000606 | 0.000692 | 0.000788 | 0.000919 | 0.001034 | 0.001034 |
| 1400  | 0.000339 | 0.000430 | 0.000546 | 0.000622 | 0.000705 | 0.000815 | 0.000907 | 0.000907 |
| 1420  | 0.000309 | 0.000391 | 0.000496 | 0.000564 | 0.000637 | 0.000730 | 0.000804 | 0.000804 |
| 1440  | 0.000281 | 0.000356 | 0.000451 | 0.000511 | 0.000575 | 0.000654 | 0.000714 | 0.000714 |
| 1460  | 0.000252 | 0.000319 | 0.000403 | 0.000456 | 0.000511 | 0.000577 | 0.000625 | 0.000625 |
| 1480  | 0.000222 | 0.000280 | 0.000354 | 0.000400 | 0.000446 | 0.000500 | 0.000537 | 0.000537 |
| 1500  | 0.000193 | 0.000244 | 0.000307 | 0.000347 | 0.000386 | 0.000429 | 0.000458 | 0.000458 |

Table 1. Ding's<sup>5</sup>  $QY$  data for graphite dust grains with radii in the range 20 to 300  $\text{\AA}$  and photon wavelengths from 9118 to 1500  $\text{\AA}$ .

Angstroms  $\lambda$   
a

|       | 500      | 700      | 1000     | 1500     | 2000     | 3000     | 5000     |
|-------|----------|----------|----------|----------|----------|----------|----------|
| 911.8 | 0.045718 | 0.040483 | 0.036134 | 0.034520 | 0.030148 | 0.027785 | 0.025657 |
| 920   | 0.044328 | 0.039271 | 0.035072 | 0.033504 | 0.029273 | 0.026980 | 0.024911 |
| 940   | 0.039606 | 0.035153 | 0.031427 | 0.030031 | 0.026273 | 0.024218 | 0.022351 |
| 960   | 0.032554 | 0.028976 | 0.025940 | 0.024809 | 0.021732 | 0.020042 | 0.018496 |
| 980   | 0.024285 | 0.021690 | 0.019447 | 0.018627 | 0.016339 | 0.015083 | 0.013925 |
| 1000  | 0.017063 | 0.015291 | 0.013730 | 0.013178 | 0.011572 | 0.010697 | 0.009888 |
| 1020  | 0.011760 | 0.010553 | 0.009489 | 0.009125 | 0.008020 | 0.007327 | 0.006875 |
| 1040  | 0.008152 | 0.007302 | 0.006569 | 0.006328 | 0.005563 | 0.005158 | 0.004782 |
| 1060  | 0.005801 | 0.005168 | 0.004645 | 0.004481 | 0.003936 | 0.003652 | 0.003290 |
| 1080  | 0.004302 | 0.003797 | 0.003404 | 0.003284 | 0.002880 | 0.002673 | 0.002483 |
| 1100  | 0.003356 | 0.002918 | 0.002603 | 0.002510 | 0.002196 | 0.002038 | 0.001893 |
| 1120  | 0.002768 | 0.002360 | 0.002089 | 0.002012 | 0.001756 | 0.001628 | 0.001512 |
| 1140  | 0.002407 | 0.002013 | 0.001762 | 0.001692 | 0.001474 | 0.001365 | 0.001267 |
| 1160  | 0.002185 | 0.001803 | 0.001556 | 0.001489 | 0.001294 | 0.001196 | 0.001109 |
| 1180  | 0.002033 | 0.001671 | 0.001424 | 0.001356 | 0.001175 | 0.001084 | 0.001004 |
| 1200  | 0.001911 | 0.001576 | 0.001328 | 0.001256 | 0.001084 | 0.000999 | 0.000924 |
| 1220  | 0.001811 | 0.001494 | 0.001246 | 0.001167 | 0.001004 | 0.000924 | 0.000853 |
| 1240  | 0.001723 | 0.001411 | 0.001164 | 0.001077 | 0.000925 | 0.000849 | 0.000783 |
| 1260  | 0.001629 | 0.001316 | 0.001076 | 0.000981 | 0.000842 | 0.000771 | 0.000710 |
| 1280  | 0.001531 | 0.001219 | 0.000991 | 0.000890 | 0.000763 | 0.000697 | 0.000640 |
| 1300  | 0.001431 | 0.001134 | 0.000919 | 0.000812 | 0.000695 | 0.000633 | 0.000580 |
| 1320  | 0.001322 | 0.001058 | 0.000857 | 0.000743 | 0.000637 | 0.000578 | 0.000529 |
| 1340  | 0.001199 | 0.000979 | 0.000792 | 0.000676 | 0.000582 | 0.000526 | 0.000480 |
| 1360  | 0.001067 | 0.000888 | 0.000716 | 0.000606 | 0.000527 | 0.000473 | 0.000431 |
| 1380  | 0.000941 | 0.000795 | 0.000638 | 0.000538 | 0.000472 | 0.000422 | 0.000384 |
| 1400  | 0.000835 | 0.000710 | 0.000571 | 0.000479 | 0.000423 | 0.000377 | 0.000342 |
| 1420  | 0.000755 | 0.000637 | 0.000516 | 0.000430 | 0.000382 | 0.000340 | 0.000308 |
| 1440  | 0.000686 | 0.000571 | 0.000466 | 0.000385 | 0.000345 | 0.000307 | 0.000277 |
| 1460  | 0.000614 | 0.000503 | 0.000412 | 0.000340 | 0.000305 | 0.000272 | 0.000245 |
| 1480  | 0.000537 | 0.000436 | 0.000356 | 0.000294 | 0.000265 | 0.000237 | 0.000213 |
| 1500  | 0.000459 | 0.000374 | 0.000305 | 0.000252 | 0.000227 | 0.000203 | 0.000183 |

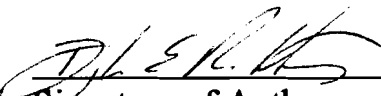
Table 2. Ding's<sup>5</sup> QY data for graphite dust grains with radii in the range 500 to 5000 Å and photon wavelengths from 9118 to 1500 Å.

|                   | $n(H)$ ( $1/m^3$ ) | $n(e)$ ( $1/m^3$ ) | T (K) |
|-------------------|--------------------|--------------------|-------|
| Cool Atomic Cloud | 2.50E+07           | 7500               | 100   |
| Warm Intercloud   | 2.50E+05           | 2500               | 8000  |

Table 3. Interstellar gas parameters for cool diffuse clouds and warm intercloud media.

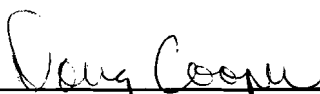


I, Douglas Edward Robertson, hereby submit this thesis to Emporia State University as partial fulfillment of the requirements for an advanced degree. I agree that the Library of the University may make it available for the use in accordance with its regulations governing materials of this type. I further agree that quoting, photocopying, or other reproduction of this document is allowed for private study, scholarship (including teaching) and research purposes of a nonprofit nature. No copying which involves potential financial gain will be allowed without written permission of the author.

  
\_\_\_\_\_  
Signature of Author

MAY 4, 1995  
\_\_\_\_\_  
Date

PHOTOELECTRIC HEATING OF INTERSTELLAR GAS  
\_\_\_\_\_  
Title of Thesis

  
\_\_\_\_\_  
Signature of Graduate Office  
Staff Member

May 5, 1995  
\_\_\_\_\_  
Date Received